
MINUN: ACCURATE ML INFERENCE ON MICROCONTROLLERS

Shikhar Jaiswal^{*1} Rahul Kiran Kranti Goli^{*2} Aayan Kumar³ Vivek Seshadri¹ Rahul Sharma¹

ABSTRACT

Running machine learning inference on tiny devices, known as TinyML, is an emerging research area. This task requires generating inference code that uses memory frugally, a task that standard ML frameworks are ill-suited for. A deployment framework for TinyML must be a) parametric in the number representation to take advantage of the emerging representations like posits, b) carefully assign high-precision to a few tensors so that most tensors can be kept in low-precision while still maintaining model accuracy, and c) avoid memory fragmentation. We describe MINUN, the first TinyML framework that holistically addresses these issues to generate efficient code for ARM microcontrollers (e.g., Arduino Uno, Due and STM32H747) that outperforms the prior TinyML frameworks.

1 INTRODUCTION

Even though memory is one of the most expensive resources, widely-used machine learning (ML) frameworks like TensorFlow and PyTorch assume the availability of plentiful memory during inference. Memory constraints are hard: exceeding the available memory by a single byte will cause a crash. Hence, these frameworks, which rely on interpreters, are unsuitable for running ML on memory-constrained devices. For example, an Arduino Uno (Banzi & Shiloh, 2014) has 2 KBs of RAM then no ML interpreter can fit in it. In this paper, we explore deployment frameworks for running ML inference on such devices.

Recently, there has been a flurry of work in the TinyML¹ space that aims to run ML on low-power embedded devices (Ghanathe et al., 2021; Kumar et al., 2020; Gopinath et al., 2019; Gupta et al., 2017; Kumar et al., 2017; Kusupati et al., 2018; Dennis et al., 2018; 2019; Saha et al., 2020; Wang et al., 2019; Lin et al., 2020; 2021). As a motivating example, consider a low-power chip embedded in the brain that can detect the onset of seizures and warn the user (Kumar et al., 2017). Animal testing of brain chips is already under way by NEURALINK (Musk, 2019). Such chips need to both perform inference locally on the device (user might be in a place with no internet connectivity) and be low-power (to avoid tissue damage caused by heat dissipation and brain surgeries for battery replacement). Since maintaining large RAMs drains batteries, these tiny devices need to have small RAMs, ranging from a few bytes to a

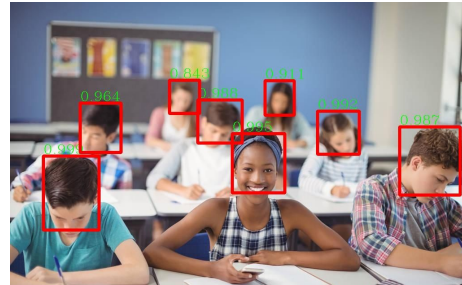


Figure 1. Face detection example.

few kilobytes (KBs). Although, the technical specifications of NEURALINK are unavailable in public domain, for reference, the microcontrollers in pacemakers in hearts have memories between 16 bytes and 10 KBs (Sharma, 2014; Jekova & Krasteva, 2004). Hence, there is a need for deployment frameworks that compile ML models to memory efficient code that can run within the specified RAM limits of the tiny devices.

Running ML inference on tiny devices is non-trivial. For example, Convolutional Neural Networks (CNNs) have millions of parameters, require MBs or GBs of memory, and are unsuitable to be run on tiny devices. Hence, we are interested in recent models targeted for tiny devices that have been specifically designed to provide good accuracy while requiring only thousands of parameters and KBs of memory (Gupta et al., 2017; Kumar et al., 2017; Kusupati et al., 2018; Saha et al., 2020), e.g., Recurrent Neural Networks (RNNs). However, even running these models on tiny devices is challenging. All such ML models use high-precision 32-bit floating-points and we want to squeeze them onto tiny devices by further reducing bitwidths. For example, suppose we want to run *face detection* (Yoo et al., 2019; He et al., 2019; Zhang et al., 2017; Zhao et al., 2019a) on a stan-

^{*}Equal contribution ¹Microsoft Research, India ²ETH Zurich, Switzerland ³UC Berkeley, USA. Correspondence to: Shikhar Jaiswal <jaiswalshikhar87@gmail.com>.

Preliminary work. Under review by the Machine Learning and Systems (MLSys) Conference. Do not distribute.

¹<https://www.tinyml.org/>

standard ARM Cortex-M class microcontroller with 256 KBs of RAM (ARM, 2021). See **Figure 1** for an example where an ML model has marked the heads in the image. The RNNPOOL (Saha et al., 2020) model provides state-of-the-art accuracy while consuming only ~ 600 KBs of RAM, which is a huge improvement over prior models, for e.g., even size-optimized architectures like MobileNetV2-SSDLite need over 3 MBs of RAM. However, this RNNPOOL model still exceeds the available memory of the 256 KB device.

An approach that has been well-studied in the literature is to compile or retrain 32-bit floating-point ML models to low bitwidth 8-bit or 2-bit or 1-bit code (Jacob et al., 2018; Nagel et al., 2019; Krishnamoorthi, 2018; Meller et al., 2019; Chen et al., 2019; Zhao et al., 2019b; Hou et al., 2019; Li et al., 2017; Gong et al., 2019; He & Fan, 2019; Zhou et al., 2018; Louizos et al., 2019; Sakr & Shanbhag, 2019; Martinez et al., 2018). However, the bitwidth required to maintain accuracy depends on the number of model parameters. In particular, it is well-known that models with fewer parameters need larger bitwidths (Fromm et al., 2018) to maintain accuracy. The techniques that use bitwidths ≤ 8 have only been shown to succeed on large models with millions of parameters. For the models of our interest, e.g., the RNNPOOL-based face detection model, even 8-bits are insufficient to maintain model accuracy (**Section 6.3**).

In the TinyML space, Tensorflow-Lite (TFLITE) (Jacob et al., 2018) converts floating-point CNNs to models that uses 8-bits for weights and 32-bits for biases; these models are then run in the TFLITE interpreter that has its own memory overheads. SEEDOT (Gopinath et al., 2019) is more expressive and compiles arbitrary models to 16-bit fixed-point C++ code that runs on bare metal. SHIFTRY (Kumar et al., 2020) goes a step further and compiles to a mixture of 8-bit and 16-bit fixed-point C++ code. Our evaluation shows that these prior frameworks are unsatisfactory when addressing the three primary subproblems of TinyML.

1.1 The Three Subproblems of TinyML

First, we need to use number representations that can both approximate the 32-bit floating-point numbers well with a smaller number of bits, and operations on which are efficiently implementable in hardware. Recently there has been a wave of new number representations (Johnson, 2018; Chen et al., 2017; Gudovskiy & Rigazio, 2017; Köster et al., 2017; Miyashita et al., 2016; Zhou et al., 2017): TFLITE’s *Zero-Skew*, Google’s *BFloat16*, NVIDIA’s *TensorFloat-32*, Microsoft’s *MSFP*, Tesla’s *CFP8* and the *posit* (Gustafson & Yonemoto, 2017; Gustafson, 2017) representation. Posits are attractive as they have better dynamic range and precision compared to floating-point. Prior frameworks for TinyML are tied to specific representations like zero-skew (Jacob et al., 2018) or fixed-point (Gopinath et al.,

2019; Kumar et al., 2020). A robust framework that remains relevant with rapidly evolving number representations must be parametric in the number representation.

Second, for each tensor², we need to decide whether to keep it in high precision or in low precision. Keeping all tensors in low precision leads to huge accuracy loss while keeping them all in high precision is wasteful memory-wise (**Section 6**). Hence, for N tensors, we have 2^N choices and need a heuristic to select a good *bitwidth assignment* that minimizes memory, while retaining model accuracy. Crucially, the decision of whether a tensor is assigned low-precision or high-precision must take into account *both* the size of the tensor, and the impact it has on the precision. No prior work provides such a technique to obtain a good bitwidth assignment. Note that TFLITE and SEEDOT use the same bitwidth assignment for all models, whereas, SHIFTRY exclusively uses accuracy to find a suitable bitwidth assignment.

Third, unlike modern CPUs, tiny devices have no hardware support for virtual memory. Therefore, *fragmentation* can quickly make a program go out of memory. Whether a program can fit in a given memory limit or not is an NP-complete bin packing problem. The solutions provided by prior works for this *memory management* problem, i.e., deciding the physical memory address at which a new tensor is allocated, are unsatisfactory: TFLITE asks programmers to manually³ manage RAM, SEEDOT uses wasteful static allocation, and SHIFTRY uses heuristics to reduce fragmentation that have no optimality guarantees. Although reusing memory for different variables has the flavor of *register allocation* (Aho et al., 2006), note that registers don’t suffer from fragmentation, which is the primary problem here.

1.2 Our Contributions

We provide a framework, MINUN⁴, that makes significant advances on all three subproblems. MINUN is the first TinyML framework which is parametric over any arbitrary number representation and we evaluate MINUN with both fixed-point and posit representations. We have designed MINUN to have a clear separation between the representation-specific and the representation-independent parts (**Section 4.1**). In contrast, the prior TinyML frameworks are extremely tied to the number representation that they work with, e.g., fixed-point for SEEDOT and SHIFTRY.

²In TinyML, it is common for all elements of a tensor to have the same bitwidth to avoid the memory overheads of book-keeping the bitwidths associated with the individual elements.

³<https://www.tensorflow.org/lite/microcontrollers#limitations>

⁴Code and datasets available at: https://github.com/krantikiran68/EdgeML/tree/shikhar_posit_vbw_haunter

For the bitwidth assignment problem, we propose a novel exploration algorithm, HAUNTER (Section 4.1), which uses both accuracy and size to produce better assignments than the accuracy-based heuristic of SHIFTRY, while being much more efficient and scalable (Section 4.2).

Finally, for RAM management, MINUN encodes the memory management problem to a bin-packing problem and solves it using Knuth’s Algorithm X (Knuth, 2000) (Section 4.3), which is guaranteed to return the optimum result albeit in exponential time. Here, our main contribution is to come up with an effective encoding and to adapt the general framework of Algorithm X to ensure a tractable runtime in practice.

In particular, for the model in Figure 1, MINUN reduces the RAM consumption from ~ 600 KBs to ~ 180 KBs, thus enabling this model to run on devices with 256 KBs of RAM. Although MINUN was not designed for large models, even on an ImageNet-scale CNN (Iandola et al., 2016), MINUN outperforms the prior TinyML frameworks (Section 6.7).

We believe that MINUN has an important role in the repertoire of techniques to reduce memory usage of ML models. We anticipate that the ML researchers will apply various techniques like structural pruning, low-rank approximation of weight matrices, novel model architectures, etc., to create models with fewer parameters and MINUN will further reduce the memory usage by keeping most of these parameters in low bitwidths. For example, the models used in our evaluation are based on novel ML architectures that keep the number of model parameters small, and MINUN further reduces the peak RAM usage by keeping most of the model parameters in lower bitwidth. Hence, the “post training quantization” of MINUN is complementary to the quantization techniques used during training.

Next, we discuss related work (Section 2) followed by an overview of MINUN (Section 3). Section 4 contains technical details, Section 5 contains implementation details and Section 6 presents our empirical results. Additional background is provided in Appendix A and a worked out example in Appendix B.

2 RELATED WORK

Running ML models with minimum resources is a vast subject and we do not attempt to survey it here. The design of new CNN architectures manually (Huang et al., 2017; Sandler et al., 2018) or automatically with Network Architecture Search (NAS) (Cai et al., 2018; Tan & Le, 2019; Shaw et al., 2019) focuses on reducing model size and compute requirements but not the peak RAM usage, which is our focus here; if the peak RAM usage exceeds the available RAM then the model fails. Techniques like pruning channels/filters (He et al., 2017) and spatial down-sampling (Saha et al., 2020)

reduce peak memory usage and are complementary to MINUN.

There are various approaches for quantization in the ML literature. In *hybrid-quantization* (Iandola et al., 2016; Jacob et al., 2018) on smartphones, each low bitwidth tensor is converted to 32-bit floating-point at runtime, computed upon in floating-point, and then converted back to low bitwidth. This approach is untenable for the models and devices that we consider because we have observed that even converting a single quantized tensor to 32-bit overflows the RAM. Apart from SHIFTRY (Kumar et al., 2020), prior papers on quantization use the trivial bitwidth assignment of mapping all tensors in large CNNs to low bitwidths (Lin et al., 2015; Hubara et al., 2016; Courbariaux & Bengio, 2016; Rastegari et al., 2016; Chen et al., 2019; Zhao et al., 2019b; Hou et al., 2019; Li et al., 2017; Gong et al., 2019; He & Fan, 2019; Zhou et al., 2018; Louizos et al., 2019; Sakr & Shanbhag, 2019; Martinez et al., 2018; Nagel et al., 2019; Krishnamoorthi, 2018; Meller et al., 2019; Jacob et al., 2018). Most of these approaches rely on retraining a low-bitwidth model, which is a computationally very expensive process. Thus, “post-training quantization” frameworks (Jacob et al., 2018; Gopinath et al., 2019; Kumar et al., 2020) like MINUN offer a distinct advantage.

MINUN is related to floating-point tuning algorithms like Precimonious (Rubio-González et al., 2013). However, their objective is completely orthogonal to the problem considered by MINUN. MINUN aims to maximize the accuracy of a program while strictly respecting the memory usage constraints, while the Precimonious algorithm aims to maximize performance (in terms of latency of execution) while strictly respecting the precision constraints. We are not aware of any floating-point heuristic tuning algorithm which has the same objectives as MINUN.

Memory management in the space of embedded devices is currently performed via wasteful static allocation, fragmentation-prone dynamic allocation, memory pools with restricted applicability, and so on. Avissar et al. (2002) use Integer Linear Programming (ILP) to generate optimal allocation schemes for a memory management problem that is different from ours and their allocations are suboptimal for the problem we consider.

MINUN can be thought of as an approximation framework for ML models. Most existing approximation frameworks map floating-point programs to other floating-point programs (Sidiroglou-Douskos et al., 2011; Rubio-González et al., 2013; Zhu et al., 2012; Schkufza et al., 2014; Baek & Chilimbi, 2010; Panchekha et al., 2015). Converters from floating-point to fixed-point that have not been designed for ML include (Darulova & Kuncak, 2014; 2017; Darulova et al., 2013; Babb et al., 1999; Brooks & Martonosi, 1999; Nayak et al., 2001; Banerjee et al., 2003; Bečvář

& Štukjunger, 2005; Menard et al., 2002; Willems, 1997).

3 COMPILER OVERVIEW

In this section, we provide a high-level overview of the MINUN compiler (Figure 2). MINUN expects as input a program written in the SHIFTRY-DSL (Kumar et al., 2020), a concise syntax for expressing operations and functions commonly used in ML models.

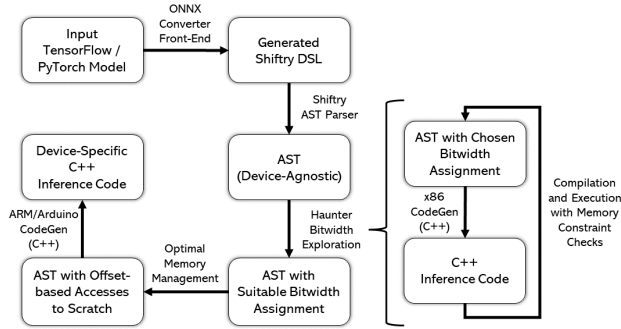


Figure 2. MINUN Overview.

The DSL code for models can either be written manually or automatically obtained by exporting TensorFlow/PyTorch models to ONNX and using MINUN’s ONNX front-end (Section 5). MINUN then parses the input program from the DSL and generates an abstract syntax tree (AST) required for HAUNTER, our bitwidth exploration strategy. HAUNTER then returns a suitable bitwidth assignment for all the tensors in the program. This is achieved by choosing an initial bitwidth assignment, generating the corresponding x86 C++ inference code for it, compiling it using GCC and executing the code for logging accuracy and memory usage, and using the logged information for making changes to the bitwidth assignment. HAUNTER ensures that user-provided memory constraints are always met during bitwidth exploration, and returns a suitable assignment which maximizes accuracy.

Then through our optimum memory management strategy, we obtain a *memory map* from RAM tensors to indices in a global *scratch* buffer, corresponding to the given bitwidth configuration. Recall that the aim of MINUN is to minimize the total size of *scratch* while ensuring that the program executes correctly.

The final device-specific C++ code is generated using a codegen pass over the AST, which also replaces all the intermediate RAM tensors, with offsets-based accesses to *scratch* on the basis of our memory map. This final C++ code is then cross-compiled (using either ARM GNU Toolchain or Arduino IDE) and executed on the microcontroller of choice. Further, we exposit the technical details, and analyze the empirical benefits of MINUN.

4 TECHNICAL DETAILS

In this section, we explain HAUNTER, analyze its complexity, and describe our memory management mechanism. A working example is provided in Appendix B and detailed algorithms used by HAUNTER are provided in Appendix C.

4.1 Bitwidth Assignment with HAUNTER

The HAUNTER algorithm works in a three-stage process, with the first stage being dependent on the number representation being considered, and the remaining two stages staying agnostic to the representation. HAUNTER uses three pieces of user-provided information - the amount of available RAM, a pair of bitwidths (*highBitwidth* and *lowBitwidth*) between which the exploration is to be commenced, and a soft limit factor that acts as a tuning parameter which can be used to make the exploration process more frugal, by choosing a soft limit < 1 . We use ρ to denote the bitwidth assignment, that maps each tensor to two possible bitwidths $\{lowBitwidth, highBitwidth\}$. Note that while we limit most discussions to 8-bit / 16-bit to simplify exposition and allow comparison, HAUNTER generalizes in a straightforward manner to exploration across various bitwidths (Section 6.8.2).

4.1.1 Preprocessing (Stage I)

This stage finds the values of data-dependent parameters that capture the runtime ranges of inputs and intermediate tensors. Examples of such parameters include the most suitable value of *es* (Section A.2) for 8-bit and 16-bit posits (since multiple *es* options are supported for these bitwidths), and scales (Section A.1) for individual tensors for fixed-point. Algorithm 4 in Appendix C succinctly describes the driver method used for obtaining these parameters for posits, where we simply pick an appropriate *es* value based on accuracy obtained with homogeneous bitwidth configurations. To determine scales of fixed-point, we use SHIFTRY’s data-driven scale assignment procedure (Kumar et al., 2020), that profiles each tensor in the floating-point version of the code by running it on a given set of inputs. This profiling information includes the minimum and maximum values observed for each tensor, and is used for assigning a suitable scale to the fixed-point tensor (Section A.1).

4.1.2 Heat-Map Generation (Stage II)

During inference on a particular data point, a “value map” stores key-value pairs, where the keys are the tensor names, and the values are the floating point values held by that tensor during execution on the provided data point. HAUNTER starts from an initial configuration where all the tensors are kept in *lowBitwidth*. In the first phase (Algorithm 5 in Appendix C), we set each promotable tensor to *highBitwidth* simultaneously, and then compile and execute the code to

obtain a “high-bitwidth value map”. We repeat the same procedure once more, by simultaneously setting each tensor to *lowBitwidth*, compiling and executing to obtain a similar “low-bitwidth value map”.

Based on these two maps, we attempt to create a “heat map” in the second phase (**Algorithm 6** in **Appendix C**), wherein, we simply calculate the absolute deviation in the representative floating-point values between the *highBitwidth* and *lowBitwidth* case for each tensor. Since keeping track of large tensors is infeasible, we simply sort the element-wise deviations in increasing order and take the 95th percentile deviation as the representative error deviation for each tensor. We define the promotability score as:

$$\text{Promotability} = \frac{\text{95th Percentile Error Deviation}}{\text{Tensor Cardinality}}$$

Here, tensor cardinality refers to the size of the tensor or the number of elements in a tensor. Sorting the tensors in decreasing order of the promotability scores provides an ordered ranking called *promotionOrder*, which prioritizes smaller-sized tensors with large error deviations to be promoted first. One could advocate the use of accuracy values as the metric to be used in place of error deviation for promotability scores. While it is a more direct metric for promoting tensors, this strategy, like SHIFTRY’s bitwidth exploration, suffers from higher computational complexity (**Section 4.2**).

4.1.3 Promotion Algorithm (Stage III)

The promotion algorithm (**Algorithm 8** in **Appendix C**) itself runs in three stages. The first stage aims to cumulatively promote all the tensors while staying within the *memoryLimit*, and also determine which tensors can potentially overshoot the provided limit. The second stage individually considers these “overshooting” tensors, by promoting them first, and then commencing the *promotionOrder*-based exploration. The final stage commences the exploration after simultaneously promoting all of these “overshooting” tensors. The final bitwidth configuration is chosen as the one minimizing the disagreement counts against the floating point code outputs, and is returned as the output of the bitwidth exploration.

4.2 Complexity Analysis

Bitwidth exploration, via HAUNTER, is the most computationally expensive block of MINUN, owing to repeated code code generation and compilation for varying bitwidth assignments, and execution calls for measuring the accuracy. While the former depends on the size of the program text of the model, the latter is determined by both the runtime of the model and the size of the dataset being considered.

We denote the amount of time required per code genera-

tion call as $\mathcal{T}_{codegen}$, and treat it as the upper bound of the code generation and compilation time required for different bitwidth configurations. We follow the same terminology for execution call latency (per example) as well, terming it $\mathcal{T}_{execution}$.

For a model of N tensors, supplied with a dataset of D samples, SHIFTRY incurs a bitwidth exploration latency of:

$$\mathcal{O}(N \times D \times \mathcal{T}_{execution} + N \times \mathcal{T}_{codegen})$$

which HAUNTER improves to (see **Section C.1**):

$$\mathcal{O}(\log N \times D \times \mathcal{T}_{execution} + N \times \log N \times \mathcal{T}_{codegen})$$

Table 3 and **Table 12** in **Appendix D** reports the empirical reduction in code generation and compilation time.

4.3 Optimum Memory Management

Once the bitwidth assignment has been computed, MINUN must allocate tensors at physical memory addresses to keep the peak RAM consumption low by maximizing the reuse of RAM locations. There are several ways to do this memory management.

Static Assignment: Tensors are pushed onto the program stack when they come in scope and popped out when they go out of scope in Last-In-First-Out (LIFO) order. This approach results in high RAM consumption as a tensor X cannot be deallocated before tensors instantiated later are deallocated, even when X is no longer live.

Dynamic Assignment: Tensors are allocated memory on the program heap, and freed when no longer needed. This approach delegates the memory management to the runtime, which may not be preferable for resource-constrained devices owing to their runtime overheads. This approach is known to be prone to fragmentation (Kumar et al., 2020), as depicted in **Figure 3**. Here, deallocating variables A and C has fragmented the memory.

Delegating Memory Management to the Compiler: Given an ML model with a fixed-sized input, tensor sizes and live ranges (range of instructions where a tensor is used and needs memory) can be known at compile time. A mapping from tensors to memory locations (or indices) on a contiguous array (*scratch*) can be computed during the code generation process itself. This reuses the memory for tensors that are no longer alive to allocate new tensors. For example, in **Figure 3**, one way to avoid fragmentation is for the compiler to map A and C to memory locations that are adjacent to each other. Computing such maps is an NP-Hard bin packing problem which can be addressed through suboptimal greedy heuristics.

Static and Dynamic Assignment methods fail to fit FAST-GRNN and RNNPOOL models for the typical RAM bud-

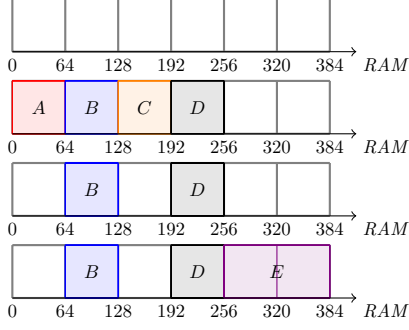


Figure 3. Fragmentation example: 1) Start with an empty RAM. 2) Allocate tensors A , B , C , and D , each of 64-bytes. 3) Later, deallocate A and C , freeing 128 bytes. 4) Then allocate E of size 128 bytes. Fragmented RAM Usage: 384 bytes, Optimal Peak RAM Usage: 256 bytes.

gets that are available with microcontrollers. Hence, we take the third approach, but unlike prior work (Kumar et al., 2020) we do not use greedy heuristics. Instead, we approach the bin-packing problem as an exact cover problem.

Definition 1 (Exact Cover): Let $\mathcal{P}(X)$ denote the power set of a set X . Given a set X and a set $S \subset \mathcal{P}(X)$, an exact cover of X is a set $S^* \subset S$ such that:

- $s_i \cap s_j = \emptyset, \forall s_i, s_j \in S^*, i \neq j$
- $\bigcup_{s_i \in S^*} s_i = X$

Consider a 2-D canvas of size $M \times I$ (where M is the memory budget in bytes along y-axis and I is the number of instructions in the program along x-axis). The smallest individual element c_i of the canvas is a square of unit area, semantically denoting a byte-sized tensor which is active only for a single instruction. For a tensor v_i active between instructions i_{start} and i_{end} , and occupying b_i bytes in memory, we can map a rectangle made of $b_i \times (i_{end} - i_{start})$ contiguous units on this canvas, occurring between i_{start} and i_{end} .

Let $\mathcal{C} = \{c_1, c_2, \dots, c_{M \times I}\}$ denote the set of all unit elements of the canvas, and $\mathcal{V} = \{v_1, v_2, \dots, v_N\}$ denote the set of all tensors in the program. Additionally, for each tensor v_i , we define a new set $\mathcal{C}_{v_i} \subset \mathcal{C}$ containing all subsets of unit elements in \mathcal{C} , which can be potential memory maps to the tensor. Hence, each individual set in \mathcal{C}_{v_i} forms a contiguous block of memory spanning the live range of v_i , and has a height of at least b_i units, as depicted in Figure 4.

Let $X = \mathcal{C} \cup \mathcal{V}$ and $S \subset \mathcal{P}(X)$ with the following constraint: $\forall s_k \in S, v_i \in \mathcal{V}[v_i \in s_k \Rightarrow s_k \setminus v_i \in \mathcal{C}_{v_i}]$

Given these sets, we solve the exact cover problem using an exponential-time, backtracking search algorithm called Algorithm X (Knuth, 2000), with the following optimizations

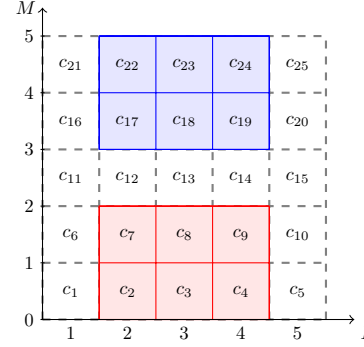


Figure 4. Example canvas with potential memory maps (in color) for a 2-byte tensor active between instructions 2 and 4. Note that each such map would form a unique element in \mathcal{C}_{v_i} for a given v_i .

to speed up the exploration:

- We use the Dancing Links Algorithm as proposed in (Knuth, 2000) to efficiently assign and unassign a tensor rectangle to a particular memory location.
- We visit the tensors in decreasing order of the area of the rectangles, as a heuristic to quickly prune out assignments causing conflicts between tensors.
- We make a coarsening assumption: all tensors are assumed to have a size as a multiple of some coarsening constant k . For example, if a program has 3 tensors of size 32, 56 and 64 bytes, then we can set $k = 32$, rounding up the sizes of the tensors as needed. Once all tensor sizes are a multiple of k , we can effectively create a canvas of size $\frac{M}{k} \times I$ instead of $M \times I$ by dividing all sizes by k , which reduces the problem size. Note that choosing $k = 1$ recovers the original formulation of the algorithm, and will always find the optimal solution, if it exists.

Our optimum memory management mechanism aims to find an exact cover for the minimum viable value of M . At each instruction, we can find minimum memory budget required for execution by tightly stacking the alive tensors at that instruction, with no gaps and no overlaps along the y-axis, and looking at height of the stack. Calculating this height for all I instructions, and picking the highest value out of them, gives us this minimum budget.

Once an exact cover is found for the minimum M , we can map a tensor from the canvas to the *scratch*, by taking its minimum y-coordinate, and using that as an offset from the starting location of the *scratch*. Notice that since M denotes the minimum viable height of the canvas, it also denotes the total size of the *scratch*. Since exact cover finds a suitable allocation within the minimum viable budget, it effectively resolves the fragmentation problem.

The proof regarding the optimality of our memory management technique reduces to the proof that Algorithm X will always find an optimum assignment if it exists, which is well-known.

5 IMPLEMENTATION DETAILS

Our framework is built on top of SHIFTRY, and has been implemented in 19K lines of Python code and 12K lines of C/C++ code. Additionally, we make use of the following set of libraries in our experiments in order to obtain arithmetic routines for different number representations:

- BFLOAT (Abadi et al., 2015) is a standalone C++ header-only sub-library implemented in the TensorFlow library, allowing conversion between FLOAT32 and BFLOAT16 types.
- SOFTPOSIT (Leong, 2020) provides posit arithmetic routines for simulating on x86-based platforms using C++. The library contains all functions expected in the Posit Standard (Group, 2018). For 8-bit posits, $es = 0$ and $es = 2$ support, and for 16-bit posits, $es = 1$ and $es = 2$ support is available. For 9-bit, 10-bit, 12-bit and 32-bit posits, only $es = 2$ support is available at the time of writing.
- GEMMLOWP (Jacob et al., 2015) is a matrix multiplication library, designed for use with “low precision” 8-bit fixed-point types. It is the library used by TFLITE’s zero-skew number representation, written in C++.

For the evaluation on large models (Section 6.7), we downloaded the pre-trained ONNX model from the public ONNX Model Zoo (Team, 2021), and implemented a Python front-end for automatically compiling ONNX models to the DSL (Section 3) programs that MINUN takes as input. In cases where certain arithmetic functions are not available for a given number representation (namely, BFLOAT16 arithmetic, and $exp(x)$ function in SOFTPOSIT), we simply convert the given representation to FLOAT32, fall back on the internal FLOAT32 arithmetic for computation, and convert the generated output to the original type. This ensures fairness of comparison against the FLOAT32 gold standard. The timeout for memory management is set as 2 hours in our evaluation. For RNNPOOL models, we use a coarsening parameter of $k = 64$, and for remaining models, we use a coarsening parameter of $k = 1$.

6 EVALUATION

We refer to MINUN parameterized with the posit representation and the fixed-point representation as MINUN-POSIT and MINUN-FIXED, respectively. We will also refer to vanilla SHIFTRY as SHIFTRY-FIXED, and our adaptation of SHIFTRY to posits as SHIFTRY-POSIT. Here, we show evaluation to justify the following claims:

1. Running ML models with low-precision 8-bit representations incurs unacceptable accuracy drops (Figure 5). Note that high-precision 16-bit representations preserve accuracy (Table 9 in Appendix D).
2. MINUN-POSIT generated code that mixes 16-bit high-precision and 8-bit low-precision matches the accuracy of 32-bit floating-point models while consuming significantly less RAM (Figure 6).
3. HAUNTER, the bitwidth assignment mechanism of MINUN, outperforms the mechanisms that are exclusively accuracy-based or exclusively size-based on both fixed-point (Table 1) and posit representations (Table 2).
4. MINUN-generated fixed-point code runs on real microcontrollers (Section 6.6).
5. For some models, using optimum memory management significantly lowers the RAM consumption compared to a standard first-fit heuristic (Section 6.7, and Table 10 and Table 11 in Appendix D).
6. Even on an ImageNet-scale model (Iandola et al., 2016), MINUN outperforms the prior TinyML frameworks (Table 4).

We compare MINUN with SHIFTRY (Kumar et al., 2020) that uses both 8-bit and 16-bit fixed-point arithmetic and TFLITE (Jacob et al., 2018) that uses 8-bit zero-skew representation. Since SEEDOT (Gopinath et al., 2019) uses 16-bit fixed-point, it is guaranteed to have worse RAM consumption than MINUN and we omit comparisons with it.

6.1 Classification Models and Datasets

We evaluate on three state-of-the-art TinyML classification models developed for resource constrained devices, namely PROTONN (Gupta et al., 2017), BONSAI (Kumar et al., 2017), and FASTGRNN (Kusupati et al., 2018). These are suitable for running on Arduino class devices, which support a minimum of 2 KBs of SRAM and 40 KBs of Flash. For fairness of evaluation, we cover the entire suite of datasets evaluated by SHIFTRY. These include CIFAR (Krizhevsky, 2009), Character Recognition (CR) (de Campos et al., 2009), USPS (Hull, 1994), Curet (Varma & Zisserman, 2005), Letter (Hsu & Lin, 2002), Ward (Yang et al., 2009) and MNIST (LeCun et al., 1998) for PROTONN and BONSAI, and DSA (Altun et al., 2010), Google (Warden, 2018), HAR (Anguita et al., 2012), MNIST (LeCun et al., 1998), USPS (Hull, 1994), Industrial (Kumar et al., 2020) and Wakeword (Kusupati et al., 2018) for FASTGRNN.

6.2 Localization Models and Datasets

RNNPOOL (Saha et al., 2020) is a new pooling layer developed for reducing the sizes of convolutional outputs, while retaining sufficient information for downstream tasks, thereby saving compute and reducing memory footprint. Using RNNPOOL, we design three face detection models

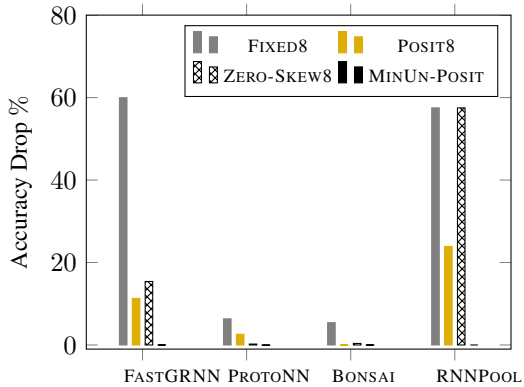


Figure 5. Accuracy/MAP drop against FLOAT32 gold standard for different models (lower is better).

(Face-A, Face-B and Face-C) for classroom/conference setting, which take as input $320 \times 240 \times 1$ monochromatic QVGA images. The Face-C model is a direct replication of the RNNPOOL-Face-M4 model introduced in (Saha et al., 2020). The architectures of these models are summarized in Table 7 in Appendix D. These RNNPOOL-based models are designed for ARM Cortex-M class devices (Jaiswal et al., 2021), which support a minimum of 256 KBs of SRAM and 1 MB of Flash. We train these models on the WIDER FACE (Yang et al., 2016) dataset and fine-tune them on SCUT-HEAD (Peng et al., 2018) dataset. For model accuracy, we evaluate the generated codes on 20% validation split (405 images) of SCUT-HEAD Part-B, and report the MAP scores (Section A.3).

6.3 Comparison With 8-Bit Baselines

We aim to justify our first claim by comparing the accuracy of models with different 8-bit number representations against the accuracy of the FLOAT32 gold standard. Figure 5 (data in Table 8 of Appendix D) shows that 8-bit representations have poor accuracy. In the case of 8-bit posits (POSIT8), we simply pick the es which empirically leads to better accuracy on a dataset. 8-bit fixed-point (FIXED8) gives the worst accuracy, 8-bit zero-skew representation of TFLITE (ZERO-SKEW8) performs better, and POSIT8 performs the best among the 8-bit representations. However, even the accuracy loss of POSIT8 is unacceptable for FASTGRNN and RNNPOOL. By using high bitwidth 16-bit posits sparingly, the accuracy drop of MINUN-POSIT is low for all models.

6.4 Comparison With 16-Bit Baselines

We compare the accuracy and RAM consumption of MINUN-POSIT against the gold-standard FLOAT32 baseline. Since 16-bit representations also offer comparable accuracy with certain models at about $2\times$ less RAM con-

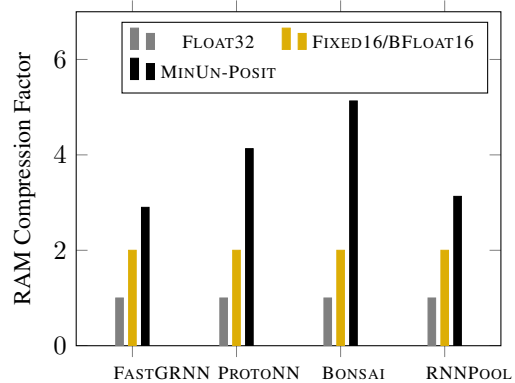


Figure 6. RAM compression relative to FLOAT32 gold standard for different models (higher is better).

sumption, we compare with 16-bit fixed-point (FIXED16) and BFLOAT16 as well. We generate our MINUN-POSIT results while ensuring that the accuracy obtained stays within 0.2% of the corresponding FLOAT32 result, for each dataset. Figure 6 summarizes our experiments, where we achieve significant reduction of $2.9\times$ – $5.1\times$ in peak RAM consumption even compared to FIXED16 or BFLOAT16, while observing only negligible differences in accuracy compared to FLOAT32. Data for Figure 6 is in Table 9 of Appendix D.

6.5 Bitwidth Assignment

We compare MINUN’s bitwidth assignment mechanism with the mechanism of SHIFTRY and other exclusively accuracy-based and exclusively size-based mechanisms in both posit and fixed-point.

In size-based baseline, we promote all tensors to higher bitwidth. Then, re-using SHIFTRY’s cumulative demotion process, we demote individual tensors, by the order of their sizes, till we arrive at a bitwidth configuration which satisfies the memory constraint being considered. Since one can initiate cumulative demotion by either considering increasing or decreasing order of tensors sizes, we report the best out of those two possible results for each dataset.

Similarly, for accuracy-based baseline, we add the same memory constraint to SHIFTRY’s demotion process. Here, we order the tensors by their individual demotion accuracies (i.e., the accuracy obtained by demoting a single tensor of interest to lower bitwidth, while keeping the remaining tensors in higher bitwidth) in decreasing order, and initiate the demotion process, and stop when we arrive at a bitwidth configuration which satisfies the limit. We also separately consider a tensor “promotion” experiment, where we initiate a cumulative promotion process after initializing all tensors to lower bitwidth, and promote tensors by the increasing order of their individual demotion accuracies, till we stay

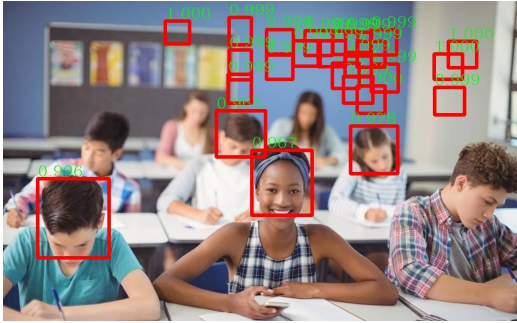


Figure 7. Example using Face-C model on SHIFTRY-FIXED.

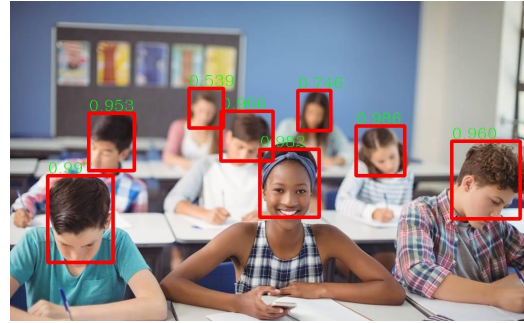


Figure 8. Example using Face-C model on MINUN-FIXED.

Table 1. Average accuracy/MAP drop of computationally expensive exploration strategies and the previous state-of-the-art on FASTGRNN, PROTONN, BONSAI and RNNPOOL models against MINUN-FIXED value.

Model	SHIFTRY-FIXED Average Drop	Accuracy-Based Average Drop	Size-Based Average Drop
FASTGRNN	0.5%	-0.2%	-0.27%
PROTONN	0.74%	0.48%	0.71%
BONSAI	0.58%	0.30%	0.25%
RNNPOOL	23.3%	-0.3%	-0.3%

within the consumption limit. Here as well, we report the best out of these two results for each dataset.

In all of our experiments, we consider the RAM consumption observed using SHIFTRY as the memory limit to be adhered to, and use soft limit factors from $\{1.0, 1.1\}$ for fixed-point, and $\{0.8, 0.9, 1.0, 1.1\}$ for our posit experiments. In case of MINUN’s result, we report the RAM consumption values while employing SHIFTRY’s first-fit greedy heuristic, as well as the optimum memory management using Algorithm X. **Table 1** (full data in **Table 10** of **Appendix D**) summarizes our experiments for fixed-point representation, with average accuracy drops against MINUN-FIXED mentioned for each exploration strategy on a per model basis. We observe better average accuracy numbers across most models and baselines while strictly staying within the same RAM constraints. **Section 6.6** shows that MINUN achieves these improvements over SHIFTRY with negligible difference in execution latency, and a significant improvement in compilation latency. Similarly, **Table 2** (full data in **Table 11** of **Appendix D**) summarizes our experiments for posits, where we compare SHIFTRY-POSIT against MINUN-POSIT. Here as well, we observe better average accuracy numbers across all models and baselines while strictly staying within the same RAM constraints. Of particular interest is fixed-point RNNPOOL where MINUN shows a 23.3% improvement in MAP score over SHIFTRY resulting in significant improvement in inference quality (see **Figure 7** and **Figure 8** for an example).

Table 2. Average accuracy/MAP drop of computationally expensive exploration strategies and the previous state-of-the-art on FASTGRNN, PROTONN, BONSAI and RNNPOOL models against MINUN-POSIT value.

Model	SHIFTRY-POSIT Average Drop	Accuracy-Based Average Drop	Size-Based Average Drop
FASTGRNN	0.58%	0.02%	0.04%
PROTONN	0.47%	0.17%	1.73%
BONSAI	0.08%	0.14%	0.06%
RNNPOOL	3%	1.2%	1.2%

Table 3. Average inference latency and compilation time drop of MINUN-FIXED against SHIFTRY-FIXED.

Model	MINUN-FIXED Inference Latency Average Drop	MINUN-FIXED Compilation Time Average Drop
FASTGRNN	0.04%	41.87%
PROTONN	-7.02%	33.25%
BONSAI	-10%	44.57%
RNNPOOL	0.03%	-2.25%

6.6 Inference Latency and Compilation Time

Note that the RAM usage and model accuracy are independent of the underlying hardware, and improvements in them (**Figure 5** and **Figure 6**) are oblivious to the microcontroller used. However, inference latency depends on the microcontroller and MINUN generates code for a variety of microcontrollers. **Table 13** in **Appendix D** provides the inference latency of running MINUN-generated fixed-point classification models on Arduino Uno, a device with 2 KB of RAM. Also see **Section A.4** for a background on microcontrollers. Further, **Table 3** (full data in **Table 12** of **Appendix D**) compares inference latency of MINUN and SHIFTRY. As expected, MINUN’s improvements in memory usage have negligible impact on the execution latency on microcontrollers. For classification and localization models, the latency is measured on Arduino Due (84 MHz, 96 KB SRAM, 512 KB Flash) and STM32H747 (240 MHz, 1 MB SRAM, 2 MB Flash) boards respectively.

We also compare the compilation time of MINUN and

SHIFTRY in [Table 3](#). For a breakup of compilation times of MINUN between bitwidth assignment and memory management, please refer to [Table 12](#) of [Appendix D](#).

6.7 Evaluation on ImageNet

[Table 4](#) evaluates MINUN-POSIT on SqueezeNet ([Iandola et al., 2016](#)) - an ImageNet-scale CNN that matches the accuracy of ALEXNET ([Krizhevsky et al., 2012](#)) while having $50\times$ smaller size. While SqueezeNet wasn’t designed for being deployed on tiny devices, we demonstrate the versatility of our framework in achieving significant RAM usage reductions even for large models through this experiment. Note that for even larger CNNs like RESNET50 and MOBILENETS, keeping all tensors in low bitwidth maintains accuracy ([Jacob et al., 2018](#)), which makes bitwidth assignment trivial. To measure accuracy, we evaluate the generated code on 48,000 RGB images spread across 1000 classes. We observe a peak RAM consumption of 1.44 MBs on the code generated by the standard first-fit ([Nutt, 2002](#)) heuristic for memory management on MINUN-POSIT, which was further reduced to 1.16 MBs on using our optimum memory management, offering a improvement of almost 20%. As evident from [Table 4](#), we achieve upto 3.81x reduction in peak RAM consumption with minimal loss in accuracy, relative to the FLOAT32 gold standard, while existing TinyML frameworks (TFLITE and SHIFTRY) fail to offer comparable reductions without leading to significant accuracy losses. In particular, MINUN has $1.9\times$ reduction in RAM consumption over SHIFTRY while obtaining 6.5% higher accuracy.

6.8 Discussion

Our evaluation shows that MINUN significantly improves the inference quality and RAM usage over SHIFTRY without degrading inference latency or compilation time. In particular, [Figure 7](#) and [Figure 8](#) show qualitatively the difference between the output of MINUN and SHIFTRY on the image in [Figure 1](#). These images show that improvements in MAP scores by MINUN translates to significantly better inference output. We discuss two approaches to improve MINUN that we evaluated but did not pursue because the gains they provided were small in practice.

6.8.1 Permitting Overflows:

For fixed-point, HAUNTER assigns bitwidths in a manner in which integer overflows are ruled out. However, this strategy is not always the best for achieving high classification accuracy. In particular, SHIFTRY permits values to overflow on some inputs to achieve higher precision on other inputs, so that the overall classification accuracy is high. While this optimization works out well in the case of fixed-point representation (where overflows are much better understood), it’s effect is hard to predict in case of other arbitrary number rep-

Table 4. Evaluation of different frameworks on SqueezeNet.

Framework	Accuracy (%)	RAM (MBs)
FLOAT32	55.02	4.42
SHIFTRY-FIXED (8-bit and 16-bit)	48.33	2.21
TFLITE-ZERO-SKEW8	45.73	1.11
MINUN-POSIT (8-bit and 16-bit)	54.81	1.16

resentations. Since HAUNTER doesn’t permit overflows, it misses out on this trade-off. This limitation is best captured through FASTGRNN model on HAR-6 dataset (details in [Table 10](#) of [Appendix D](#)), where the generated model takes a hit of almost 2% compared to other strategies, and is the only cause of the average accuracy drops being negative for FASTGRNN models in [Table 1](#).

6.8.2 Generalization to More Bitwidth Options:

HAUNTER decides between two bitwidths, *lowBitwidth* and *highBitwidth*. It is plausible that if there are more bitwidth options then HAUNTER can generate even better code. Having k bitwidth options leads to a total of k^N possible bitwidth assignments, where N is the number of tensors in the program. In general, adding more bitwidth options directly into the algorithm blows up the search space and leads to many code executions, making MINUN painfully slow. We experimented with three bitwidths (8, 12 and 16) for posits, but did not find any tangible benefit in terms of accuracy in our experiments compared to two bitwidth options of (8 and 16) or (8 and 12) or (12 and 16) cases, depending on specific models.

As such, we chose a much simpler strategy in [Table 9](#). Given $B = \{8, 9, 10, 12, 16\}$ options for bitwidths, we generated $|B|$ homogeneous bitwidth codes (one for each option) and ordered the bitwidths by the accuracy/MAP obtained on their corresponding codes. Out of these sorted bitwidths, we simply chose the two options between which the 32-bit floating point accuracy lied, as the *lowBitwidth* and *highBitwidth* respectively. In situations where there was a tie in accuracy between multiple options for *lowBitwidth* or *highBitwidth*, we simply picked the lowest of the tied bitwidth options. In total, these only require $|B|$ additional code generations and executions, which is affordable since $|B| = 5$ is small.

7 CONCLUSION

MINUN is the first TinyML framework which is parametric on number representation, generates a bitwidth assignment automatically taking into account both the size of the tensors and their impact on accuracy, and performs optimum memory management. Our evaluation shows that MINUN significantly outperforms state-of-the-art TinyML frameworks in accuracy and RAM consumption.

REFERENCES

- Abadi, M., Barham, P., Chen, J., Chen, Z., Davis, A., Dean, J., Devin, M., Ghemawat, S., Irving, G., Isard, M., Kudlur, M., Levenberg, J., Monga, R., Moore, S., Murray, D. G., Steiner, B., Tucker, P., Vasudevan, V., Warden, P., Wicke, M., Yu, Y., and Zheng, X. Tensorflow: Large-scale machine learning on heterogeneous systems. <https://github.com/tensorflow/tensorflow/blob/master/tensorflow/core/framework/bfloat16.cc>, 2015.
- Aho, A. V., Lam, M. S., Sethi, R., and Ullman, J. D. *Compilers: Principles, Techniques, and Tools (2nd Edition)*. Addison-Wesley Longman Publishing Co., Inc., USA, 2006. ISBN 0321486811.
- Altun, K., Barshan, B., and Tunçel, O. Comparative study on classifying human activities with miniature inertial and magnetic sensors. *Pattern Recognition*, 43(10):3605–3620, 2010. URL <https://archive.ics.uci.edu/ml/datasets/Daily+and+Sports+Activities>.
- Anguita, D., Ghio, A., Oneto, L., Parra, X., and Reyes-Ortiz, J. L. Human activity recognition on smartphones using a multiclass hardware-friendly support vector machine. In *Proceedings of the 4th International Conference on Ambient Assisted Living and Home Care, IWAAL'12*, pp. 216–223, Berlin, Heidelberg, 2012. Springer-Verlag. ISBN 9783642353949. URL <https://archive.ics.uci.edu/ml/datasets/human+activity+recognition+using+smartphones>.
- ARM. Arm cortex-m official website. <https://developer.arm.com/ip-products/processors/cortex-m>, 2021.
- Avissar, O., Barua, R., and Stewart, D. An optimal memory allocation scheme for scratch-pad-based embedded systems. *ACM Trans. Embed. Comput. Syst.*, 1(1):6–26, nov 2002. ISSN 1539-9087. doi: 10.1145/581888.581891. URL <https://doi.org/10.1145/581888.581891>.
- Babb, J., Rinard, M. C., Moritz, C. A., Lee, W., Frank, M. I., Barua, R., and Amarasinghe, S. P. Parallelizing applications into silicon. In *7th IEEE Symposium on Field-Programmable Custom Computing Machines (FCCM '99), 21-23 April 1999, Napa, CA, USA*, pp. 70, Napa, CA, USA, 1999. IEEE. doi: 10.1109/FPGA.1999.803669.
- Baek, W. and Chilimbi, T. M. Green: a framework for supporting energy-conscious programming using controlled approximation. In *Proceedings of the 2010 ACM SIGPLAN Conference on Programming Language Design and Implementation, PLDI 2010, Toronto, Ontario, Canada, June 5-10, 2010*, pp. 198–209, New York, NY, USA, 2010. Association for Computing Machinery. doi: 10.1145/1809028.1806620.
- Banerjee, P., Bagchi, D., Haldar, M., Nayak, A., Kim, V., and Uribe, R. Automatic conversion of floating point MATLAB programs into fixed point FPGA based hardware design. In *11th Annual IEEE Symposium on Field-Programmable Custom Computing Machines, 2003. FCCM 2003.*, pp. 263–264, Los Alamitos, CA, USA, April 2003. IEEE Computer Society. doi: 10.1109/FPGA.2003.1227262.
- Banzi, M. and Shiloh, M. *Getting started with Arduino: the open source electronics prototyping platform*. Maker Media, Inc., 2014.
- Bečvář, M. and Štukjunger, P. Fixed-point arithmetic in FPGA. *Acta Polytechnica*, 45(2), 2005.
- Brooks, D. M. and Martonosi, M. Dynamically exploiting narrow width operands to improve processor power and performance. In *Proceedings of the Fifth International Symposium on High-Performance Computer Architecture, Orlando, FL, USA, January 9-12, 1999*, pp. 13–22, New York, NY, USA, 1999. Association for Computing Machinery.
- Cai, H., Zhu, L., and Han, S. Proxylessnas: Direct neural architecture search on target task and hardware. *arXiv preprint arXiv:1812.00332*, 2018.
- Chen, S., Wang, W., and Pan, S. J. Metaquant: Learning to quantize by learning to penetrate non-differentiable quantization. In Wallach, H., Larochelle, H., Beygelzimer, A., d'Alché-Buc, F., Fox, E., and Garnett, R. (eds.), *Advances in Neural Information Processing Systems 32*, pp. 3916–3926. Curran Associates, Inc., 2019. URL <http://papers.nips.cc/paper/8647-metaquant-learning-to-quantize-by-learning-to-pen.pdf>.
- Chen, X., Hu, X., Zhou, H., and Xu, N. Fxpnet: Training a deep convolutional neural network in fixed-point representation. In *2017 International Joint Conference on Neural Networks, IJCNN 2017, Anchorage, AK, USA, May 14-19, 2017*, pp. 2494–2501. IEEE, 2017. doi: 10.1109/IJCNN.2017.7966159.
- Courbariaux, M. and Bengio, Y. Binarynet: Training deep neural networks with weights and activations constrained to +1 or -1. *CoRR*, abs/1602.02830, 2016. URL <http://arxiv.org/abs/1602.02830>.

- Darulova, E. and Kuncak, V. Sound compilation of reals. In *The 41st Annual ACM SIGPLAN-SIGACT Symposium on Principles of Programming Languages, POPL '14, San Diego, CA, USA, January 20-21, 2014*, pp. 235–248, New York, NY, USA, 2014. Association for Computing Machinery. doi: 10.1145/2535838.2535874.
- Darulova, E. and Kuncak, V. Towards a compiler for reals. *ACM Trans. Program. Lang. Syst.*, 39(2):8:1–8:28, March 2017. ISSN 0164-0925. doi: 10.1145/3014426. URL <http://doi.acm.org/10.1145/3014426>.
- Darulova, E., Kuncak, V., Majumdar, R., and Saha, I. Synthesis of fixed-point programs. In *Proceedings of the Eleventh ACM International Conference on Embedded Software, EMSOFT '13*, pp. 22:1–22:10, Piscataway, NJ, USA, 2013. IEEE Press. ISBN 978-1-4799-1443-2. URL <http://dl.acm.org/citation.cfm?id=2555754.2555776>.
- de Campos, T. E., Babu, B. R., and Varma, M. Character recognition in natural images. In *VISAPP 2009 - Proceedings of the Fourth International Conference on Computer Vision Theory and Applications, Lisboa, Portugal, February 5-8, 2009 - Volume 2*, pp. 273–280, Portugal, 2009. INSTICC Press. URL https://www.researchgate.net/publication/221416071_Character_Recognition_in_Natural_Images.
- Dennis, D., Pabbaraju, C., Simhadri, H. V., and Jain, P. Multiple instance learning for efficient sequential data classification on resource-constrained devices. In *Proceedings of the Thirty-first Annual Conference on Neural Information Processing Systems (NeurIPS)*, pp. 10976–10987, 2018. URL [all_papers/DennisPSJ18.pdf](http://papers.nips.cc/paper_files/paper/2018/file/DennisPSJ18.pdf). [slides/DennisPSJ18.pdf](http://papers.nips.cc/paper_files/paper/2018/file/DennisPSJ18.pdf).
- Dennis, D., Acar, D. A. E., Mandikal, V., Sadasivan, V. S., Simhadri, H. V., Saligrama, V., and Jain, P. Shallow rnn: Accurate time-series classification on resource constrained devices. In *Proceedings of the Thirty-second Annual Conference on Neural Information Processing Systems (NeurIPS)*, 2019.
- Fromm, J., Patel, S., and Philipose, M. Heterogeneous bitwidth binarization in convolutional neural networks. *CoRR*, abs/1805.10368, 2018. URL <http://arxiv.org/abs/1805.10368>.
- Ghanathe, N. P., Seshadri, V., Sharma, R., Wilton, S., and Kumar, A. MAFIA: machine learning acceleration on fpga for iot applications. In *31st International Conference on Field-Programmable Logic and Applications, FPL 2021, Dresden, Germany, August 30 - Sept. 3, 2021*, pp. 347–354, 2021.
- Gong, R., Liu, X., Jiang, S., Li, T., Hu, P., Lin, J., Yu, F., and Yan, J. Differentiable soft quantization: Bridging full-precision and low-bit neural networks. In *The IEEE International Conference on Computer Vision (ICCV)*, October 2019. doi: 10.1109/ICCV.2019.00495.
- Gopinath, S., Ghanathe, N., Seshadri, V., and Sharma, R. Compiling kb-sized machine learning models to tiny iot devices. In *Proceedings of the 40th ACM SIGPLAN Conference on Programming Language Design and Implementation (PLDI)*, pp. 79–95, New York, NY, USA, 2019. Association for Computing Machinery. URL <https://www.microsoft.com/en-us/research/uploads/prod/2018/10/pldi19-SeeDot.pdf>.
- Group, P. W. Posit standard documentation. https://posithub.org/docs/posit_standard.pdf, 2018.
- Gudovskiy, D. A. and Rigazio, L. Shiftcnn: Generalized low-precision architecture for inference of convolutional neural networks. *CoRR*, abs/1706.02393, 2017. URL https://www.researchgate.net/publication/317419072_ShiftCNN_Generalized_Low-Precision_Architecture_for_Inference_of_Convolutional_Neural_Networks.
- Gupta, C., Suggala, A. S., Goyal, A., Simhadri, H. V., Paranjape, B., Kumar, A., Goyal, S., Udupa, R., Varma, M., and Jain, P. ProtoNN: compressed and accurate kNN for resource-scarce devices. In *International Conference on Machine Learning*, pp. 1331–1340, International Convention Centre, Sydney, Australia, 2017. PMLR. URL <https://dl.acm.org/doi/10.5555/3305381.3305519>.
- Gustafson and Yonemoto. Beating floating point at its own game: Posit arithmetic. *Supercomput. Front. Innov.: Int. J.*, 4(2):71–86, June 2017. ISSN 2409-6008. doi: 10.14529/jsfi170206. URL <https://doi.org/10.14529/jsfi170206>.
- Gustafson, J. Posit arithmetic. 2017. URL <https://posithub.org/docs/Posits4.pdf>.
- He, Y., Zhang, X., and Sun, J. Channel pruning for accelerating very deep neural networks. In *IEEE International Conference on Computer Vision, ICCV 2017, Venice, Italy, October 22-29, 2017*, pp. 1398–1406, 2017.
- He, Y., Xu, D., Wu, L., Jian, M., Xiang, S., and Pan, C. Lffd: A light and fast face detector for edge devices. In *arXiv:1904.10633*, 2019.

- He, Z. and Fan, D. Simultaneously optimizing weight and quantizer of ternary neural network using truncated gaussian approximation. In *The IEEE Conference on Computer Vision and Pattern Recognition (CVPR)*, June 2019. URL <https://arxiv.org/abs/1810.01018>.
- Hou, L., Zhu, J., Kwok, J., Gao, F., Qin, T., and Liu, T.-Y. Normalization helps training of quantized lstm. In Wallach, H., Larochelle, H., Beygelzimer, A., d'Alché-Buc, F., Fox, E., and Garnett, R. (eds.), *Advances in Neural Information Processing Systems 32*, pp. 7346–7356. Curran Associates, Inc., 2019. URL <http://papers.nips.cc/paper/8954-normalization-helps-training-of-quantized-lstm.pdf>.
- Hsu, C.-W. and Lin, C.-J. A comparison of methods for multiclass support vector machines. *IEEE transactions on Neural Networks*, 13(2):415–425, 2002. doi: 10.1109/72.991427.
- Huang, G., Liu, Z., Van Der Maaten, L., and Weinberger, K. Q. Densely connected convolutional networks. In *Proceedings of the IEEE conference on computer vision and pattern recognition*, pp. 4700–4708, 2017.
- Hubara, I., Courbariaux, M., Soudry, D., El-Yaniv, R., and Bengio, Y. Binarized neural networks. In Lee, D. D., Sugiyama, M., Luxburg, U. V., Guyon, I., and Garnett, R. (eds.), *Advances in Neural Information Processing Systems 29*, pp. 4107–4115. Curran Associates, Inc., 2016. URL <http://papers.nips.cc/paper/6573-binarized-neural-networks.pdf>.
- Hull, J. J. A database for handwritten text recognition research. *IEEE Transactions on pattern analysis and machine intelligence*, 16(5):550–554, 1994. doi: 10.1109/34.291440.
- Iandola, F. N., Moskewicz, M. W., Ashraf, K., Han, S., Dally, W. J., and Keutzer, K. Squeezenet: Alexnet-level accuracy with 50x fewer parameters and <1mb model size. *CoRR*, abs/1602.07360, 2016. URL <https://arxiv.org/abs/1602.07360v1>.
- IEEE. Ieee standard for floating-point arithmetic. *IEEE Std 754-2019 (Revision of IEEE 754-2008)*, pp. 1–84, 2019. doi: 10.1109/IEEESTD.2019.8766229.
- Jacob, B., Warden, P., Wang, M., Andersen, D., Chociej, M., Tunney, J., J. Matthews, M., White, M., Sivakumar, S., Marcovich, S., Efe Guney, M., Knepper, S., Gouicem, M., Winterton, R., Mansell, D., Gal, A., Frunze, A., and Frunze, A. gemmlowp: a small self-contained low-precision gemm library. <https://github.com/google/gemmlowp>, 2015.
- Jacob, B., Kligys, S., Chen, B., Zhu, M., Tang, M., Howard, A., Adam, H., and Kalenichenko, D. Quantization and training of neural networks for efficient integer-arithmetic-only inference. In *Proceedings of the IEEE Conference on Computer Vision and Pattern Recognition (CVPR)*, June 2018.
- Jaiswal, S., Saha, O., Kumar, A., Simhadri, H. V., Jain, P., and Sharma, R. Enabling accurate computer vision on tiny microcontrollers with rnnpool operator and seedot compiler, 2021. URL <https://towardsdatascience.com/enabling-accurate-computer-vision-on-tiny-microcontrollers>.
- Jekova, I. and Krasteva, V. Real time detection of ventricular fibrillation and tachycardia. *Physiological measurement*, 25:1167–78, 11 2004. doi: 10.1088/0967-3334/25/5/007.
- Johnson, J. Rethinking floating point for deep learning. *CoRR*, abs/1811.01721, 2018. URL <https://arxiv.org/abs/1811.01721>.
- Knuth, D. E. Dancing links. *CoRR*, abs/cs/0011047, 2000. URL <https://arxiv.org/abs/cs/0011047>.
- Köster, U., Webb, T., Wang, X., Nassar, M., Bansal, A. K., Constable, W., Elibol, O., Hall, S., Hornof, L., Khosrowshahi, A., Kloss, C., Pai, R. J., and Rao, N. Flexpoint: An adaptive numerical format for efficient training of deep neural networks. *CoRR*, abs/1711.02213, 2017. URL <https://arxiv.org/abs/1711.02213>.
- Krishnamoorthi, R. Quantizing deep convolutional networks for efficient inference: A whitepaper. *CoRR*, abs/1806.08342, 2018. URL <https://arxiv.org/abs/1806.08342>.
- Krizhevsky, A. Learning multiple layers of features from tiny images. Technical report, Citeseer, 2009.
- Krizhevsky, A., Sutskever, I., and Hinton, G. E. Imagenet classification with deep convolutional neural networks. In *Advances in Neural Information Processing Systems 25: 26th Annual Conference on Neural Information Processing Systems 2012. Proceedings of a meeting held December 3-6, 2012, Lake Tahoe, Nevada, United States.*, pp. 1106–1114, 2012. URL <http://papers.nips.cc/paper/4824-imagenet-classification-with-deep-convolutional-neural-networks>.
- Kumar, A., Goyal, S., and Varma, M. Resource-efficient Machine Learning in 2 KB RAM for the Internet of Things. In *International Conference on Machine Learning*, pp. 1935–1944, International Convention Centre, Sydney, Australia, 2017. PMLR. URL <https://dl.acm.org/doi/10.5555/3305381.3305581>.

- Kumar, A., Seshadri, V., and Sharma, R. Shiftry: Rnn inference in 2kb of ram. *Proc. ACM Program. Lang.*, 4(OOPSLA), November 2020. doi: 10.1145/3428250. URL <https://doi.org/10.1145/3428250>.
- Kusupati, A., Singh, M., Bhatia, K., Kumar, A., Jain, P., and Varma, M. Fastgrnn: A fast, accurate, stable and tiny kilobyte sized gated recurrent neural network. In *Proceedings of the Thirty-first Annual Conference on Neural Information Processing Systems (NeurIPS)*, pp. 9031–9042, 2018. URL <https://dl.acm.org/doi/10.5555/3327546.3327577>.
- LeCun, Y., Bottou, L., Bengio, Y., and Haffner, P. Gradient-based learning applied to document recognition. *Proceedings of the IEEE*, 86(11):2278–2324, 1998. doi: 10.1109/5.726791.
- Leong, S. H. Softposit. <https://gitlab.com/cerlane/SoftPosit>, 03 2020.
- Li, H., De, S., Xu, Z., Studer, C., Samet, H., and Goldstein, T. Training quantized nets: A deeper understanding. In Guyon, I., Luxburg, U. V., Bengio, S., Wallach, H., Fergus, R., Vishwanathan, S., and Garnett, R. (eds.), *Advances in Neural Information Processing Systems 30*, pp. 5811–5821. Curran Associates, Inc., 2017. URL <http://papers.nips.cc/paper/7163-training-quantized-nets-a-deeper-understanding.pdf>.
- Lin, J., Chen, W.-M., Cohn, J., Gan, C., and Han, S. Mcunet: Tiny deep learning on iot devices. In *Annual Conference on Neural Information Processing Systems (NeurIPS)*, 2020.
- Lin, J., Chen, W.-M., Cai, H., Gan, C., and Han, S. Mcunetv2: Memory-efficient patch-based inference for tiny deep learning. In *Annual Conference on Neural Information Processing Systems (NeurIPS)*, 2021.
- Lin, Z., Courbariaux, M., Memisevic, R., and Bengio, Y. Neural networks with few multiplications. *CoRR*, abs/1510.03009, 2015. URL <http://arxiv.org/abs/1510.03009>.
- Louizos, C., Reisser, M., Blankevoort, T., Gavves, E., and Welling, M. Relaxed quantization for discretized neural networks. In *International Conference on Learning Representations*, 2019. URL <https://openreview.net/forum?id=HkxjYoCqKX>.
- Martinez, J., Zakhmi, S., Hoos, H. H., and Little, J. J. Lsq++: Lower running time and higher recall in multi-codebook quantization. In *The European Conference on Computer Vision (ECCV)*, September 2018. URL https://openaccess.thecvf.com/content_ECCV_2018/papers/Julieta_Martinez_LSQ_lower_runtime_ECCV_2018_paper.pdf.
- Meller, E., Finkelstein, A., Almog, U., and Grobman, M. Same, same but different - recovering neural network quantization error through weight factorization. *CoRR*, abs/1902.01917, 2019. URL <https://arxiv.org/abs/1902.01917>.
- Menard, D., Chillet, D., Charot, F., and Sentieys, O. Automatic Floating-point to Fixed-point Conversion for DSP Code Generation. In *Proceedings of the 2002 International Conference on Compilers, Architecture, and Synthesis for Embedded Systems, CASES '02*, pp. 270–276, New York, NY, USA, 2002. Association for Computing Machinery. ISBN 1-58113-575-0. doi: 10.1145/581630.581674. URL <http://doi.acm.org/10.1145/581630.581674>.
- Miyashita, D., Lee, E. H., and Murmann, B. Convolutional neural networks using logarithmic data representation. *CoRR*, abs/1603.01025, 2016. URL <https://arxiv.org/abs/1603.01025>.
- Musk, E. An integrated brain-machine interface platform with thousands of channels. *J Med Internet Res*, 21(10):e16194, Oct 2019. ISSN 1438-8871. doi: 10.2196/16194. URL <http://www.jmir.org/2019/10/e16194/>.
- Nagel, M., van Baalen, M., Blankevoort, T., and Welling, M. Data-free quantization through weight equalization and bias correction. In *2019 IEEE/CVF International Conference on Computer Vision, ICCV 2019, Seoul, Korea (South), October 27 - November 2, 2019*, pp. 1325–1334. IEEE, 2019. URL https://openaccess.thecvf.com/content_ICCV_2019/papers/Nagel_Data-Free_Quantization_Through_Weight_Equalization_and_Bias_Correction_ICCV_2019_paper.pdf.
- Nayak, A., Haldar, M., Choudhary, A. N., and Banerjee, P. Precision and error analysis of MATLAB applications during automated hardware synthesis for FPGAs. In *Proceedings of the Conference on Design, Automation and Test in Europe, DATE 2001, Munich, Germany, March 12-16, 2001*, pp. 722–728, 2001. doi: 10.1109/DATE.2001.915108.
- Nutt, G. J. *Operating Systems: A Modern Perspective*. Modern Perspective, Lab Update. Addison Wesley, 2002. ISBN 9780201612431. URL <https://books.google.co.in/books?id=AHBGAAAAYAAJ>.
- Pancheekha, P., Sanchez-Stern, A., Wilcox, J. R., and Tatlock, Z. Automatically improving accuracy for floating point expressions. In *Proceedings of the 36th ACM SIGPLAN*

- Conference on Programming Language Design and Implementation, Portland, OR, USA, June 15-17, 2015*, pp. 1–11, 2015.
- Peng, D., Sun, Z., Chen, Z., Cai, Z., Xie, L., and Jin, L. Detecting heads using feature refine net and cascaded multi-scale architecture. *CoRR*, abs/1803.09256, 2018. URL <http://arxiv.org/abs/1803.09256>.
- Rastegari, M., Ordonez, V., Redmon, J., and Farhadi, A. Xnor-net: Imagenet classification using binary convolutional neural networks. *CoRR*, abs/1603.05279, 2016. URL <http://arxiv.org/abs/1603.05279>.
- Rubio-González, C., Nguyen, C., Nguyen, H. D., Demmel, J., Kahan, W., Sen, K., Bailey, D. H., Iancu, C., and Hough, D. Precimonious: Tuning assistant for floating-point precision. In *Proceedings of the International Conference on High Performance Computing, Networking, Storage and Analysis, SC '13*, pp. 27:1–27:12, New York, NY, USA, 2013. Association for Computing Machinery. ISBN 978-1-4503-2378-9. doi: 10.1145/2503210.2503296. URL <http://doi.acm.org/10.1145/2503210.2503296>.
- Saha, O., Kusupati, A., Simhadri, H. V., Varma, M., and Jain, P. Rnnpool: Efficient non-linear pooling for ram constrained inference. In *Advances in Neural Information Processing Systems*, December 2020.
- Sakr, C. and Shanbhag, N. Per-tensor fixed-point quantization of the back-propagation algorithm. In *International Conference on Learning Representations*, 2019. URL <https://openreview.net/forum?id=rkxaNjA9Ym>.
- Sandler, M., Howard, A., Zhu, M., Zhmoginov, A., and Chen, L.-C. Mobilenetv2: Inverted residuals and linear bottlenecks. In *Proceedings of the IEEE conference on computer vision and pattern recognition*, pp. 4510–4520, 2018.
- Schkufza, E., Sharma, R., and Aiken, A. Stochastic optimization of floating-point programs with tunable precision. In *ACM SIGPLAN Conference on Programming Language Design and Implementation, PLDI '14, Edinburgh, United Kingdom - June 09 - 11, 2014*, pp. 53–64, 2014. doi: 10.1145/2666356.2594302.
- Sharma, A. A. A consolidated review on embedded microcontrollers for pace maker applications. In *The 2014 International Conference on Embedded Systems and Applications*, 2014.
- Shaw, A., Hunter, D., Landola, F., and Sidhu, S. Squeezenas: Fast neural architecture search for faster semantic segmentation. In *Proceedings of the IEEE/CVF International Conference on Computer Vision Workshops*, pp. 0–0, 2019.
- Sidirolou-Douskos, S., Misailovic, S., Hoffmann, H., and Rinard, M. Managing performance vs. accuracy trade-offs with loop perforation. In *Proceedings of the 19th ACM SIGSOFT Symposium and the 13th European Conference on Foundations of Software Engineering, ESEC/FSE '11*, pp. 124–134, New York, NY, USA, 2011. Association for Computing Machinery. ISBN 978-1-4503-0443-6. doi: 10.1145/2025113.2025133. URL <http://doi.acm.org/10.1145/2025113.2025133>.
- Tan, M. and Le, Q. Efficientnet: Rethinking model scaling for convolutional neural networks. In *International Conference on Machine Learning*, pp. 6105–6114. PMLR, 2019.
- Team, O. D. Onnx model zoo, 2021. URL <https://github.com/onnx/models/>.
- Varma, M. and Zisserman, A. A statistical approach to texture classification from single images. *International journal of computer vision*, 62(1-2):61–81, 2005. doi: 10.1023/B:VISI.0000046589.39864.ee.
- Wang, K., Liu, Z., Lin, Y., Lin, J., and Han, S. Haq: Hardware-aware automated quantization with mixed precision. In *Proceedings of the IEEE/CVF Conference on Computer Vision and Pattern Recognition*, pp. 8612–8620, 2019.
- Warden, P. Speech commands: A dataset for limited-vocabulary speech recognition, 2018.
- Willems, M. Fridge : Floating-point programming of fixed-point digital signal processors. *Proc. International Conference on Signal Processing Applications and Technology 1997 (ICSPAT-97), Sept., 1997*. URL <https://ci.nii.ac.jp/naid/10018558547/en/>.
- Yang, J., Li, Y., Tian, Y., Duan, L., and Gao, W. Group-sensitive multiple kernel learning for object categorization. In *Computer Vision, 2009 IEEE 12th International Conference on*, pp. 436–443, Kyoto, Japan, 2009. IEEE. doi: 10.1109/ICCV.2009.5459172.
- Yang, S., Luo, P., Loy, C. C., and Tang, X. Wider face: A face detection benchmark. In *IEEE Conference on Computer Vision and Pattern Recognition (CVPR)*, 2016.
- Yoo, Y. J., Han, D., and Yun, S. EXTD: extremely tiny face detector via iterative filter reuse. *CoRR*, abs/1906.06579, 2019. URL <http://arxiv.org/abs/1906.06579>.

- Zhang, S., Zhu, X., Lei, Z., Shi, H., Wang, X., and Li, S. Z. Faceboxes: A cpu real-time face detector with high accuracy. In *2017 IEEE International Joint Conference on Biometrics (IJCBI)*, pp. 1–9. IEEE, 2017.
- Zhao, X., Liang, X., Zhao, C., Tang, M., and Wang, J. Real-time multi-scale face detector on embedded devices. *Sensors*, 19(9), 2019a. ISSN 1424-8220. doi: 10.3390/s19092158. URL <https://www.mdpi.com/1424-8220/19/9/2158>.
- Zhao, Y., Gao, X., Bates, D., Mullins, R., and Xu, C.-Z. Focused quantization for sparse cnns. In Wallach, H., Larochelle, H., Beygelzimer, A., d'Alché-Buc, F., Fox, E., and Garnett, R. (eds.), *Advances in Neural Information Processing Systems 32*, pp. 5584–5593. Curran Associates, Inc., 2019b. URL <http://papers.nips.cc/paper/8796-focused-quantization-for-sparse-cnns.pdf>.
- Zhou, A., Yao, A., Guo, Y., Xu, L., and Chen, Y. Incremental network quantization: Towards lossless cnns with low-precision weights. In *5th International Conference on Learning Representations, ICLR 2017, Toulon, France, April 24-26, 2017, Conference Track Proceedings*. OpenReview.net, 2017. URL <https://arxiv.org/abs/1702.03044v2>.
- Zhou, A., Yao, A., Wang, K., and Chen, Y. Explicit loss-error-aware quantization for low-bit deep neural networks. In *The IEEE Conference on Computer Vision and Pattern Recognition (CVPR)*, June 2018. URL https://openaccess.thecvf.com/content_cvpr_2018/papers/Zhou_Explicit_Loss-Error-Aware_Quantization_CVPR_2018_paper.pdf.
- Zhu, Z. A., Misailovic, S., Kelner, J. A., and Rinard, M. Randomized accuracy-aware program transformations for efficient approximate computations. In *Proceedings of the 39th Annual ACM SIGPLAN-SIGACT Symposium on Principles of Programming Languages, POPL '12*, pp. 441–454, New York, NY, USA, 2012. Association for Computing Machinery. ISBN 978-1-4503-1083-3. doi: 10.1145/2103621.2103710.

A PRELIMINARIES

In this section, we discuss the terminology from fixed-point representation, posit representation, machine learning and computer vision problems, and microcontrollers.

A.1 Fixed-Point Representation

In standard fixed-point arithmetic, a real number r is stored as the b -bit signed integer $\lfloor r \times 2^s \rfloor_b$, where s is a predetermined integer called the *scale* and b is termed as the *bitwidth* of the representation. As an example, consider the real number $r = 1.6181$:

$$\begin{aligned} r = 1.6181 &= 1.6181 \times \frac{2^{14}}{2^{14}} \approx \frac{\lfloor 1.6181 \times 2^{14} \rfloor}{2^{14}} \\ &= 26510 \times 2^{-14} \end{aligned} \quad (1)$$

To represent 1.6181 in fixed-point arithmetic, we store the 16-bit integer 26510, associated with the scale of 14. The interpreted real value would be $26510 \times 2^{-14} \approx 1.61804$, which is a close approximation of the original value.

For any real number and a given bitwidth, there is an optimum scale for the fixed-point representation; in the example above, given a 16-bit integer representation, 14 is the optimum scale for 1.6181, as using a scale of 15 or above causes integer overflow, and using a scale of 13 or below leads to more imprecise results.

A generalization of the above approach is the ‘‘zero-skew’’ quantization scheme by TFLITE (Jacob et al., 2018). Here, a real number r is stored in the following manner:

$$r = S(q_b - Z) \quad (2)$$

where S is an arbitrary positive real number, termed as the skew, and Z is the quantized value of 0, termed as the zero-point, expressed in the same type as the b -bit unsigned integer q_b . Let us assume that we wish to represent a uniformly sampled real from the range $[-2, 2]$ in 8-bits. Hence, by choosing $r = 1.6181$, $S = \frac{\text{Variable Range}}{\text{uint8 Range}} = \frac{4}{255} \approx 0.015686$ and $Z = -\frac{\text{Variable Range Infimum}}{S} \approx 128$, we obtain q as:

$$q_8 = \left\lfloor \frac{1.6181}{0.015686} \right\rfloor + 128 \approx 231 \quad (3)$$

Substituting these approximations back into equation (1) gives us the interpreted value 1.6157.

The skew and the zero-point are colloquially referred to as quantization parameters. All values in a tensor use a unique set of quantization parameters. A higher bitwidth preserves more precision, as long as the underlying integer does not overflow due to a high scale.

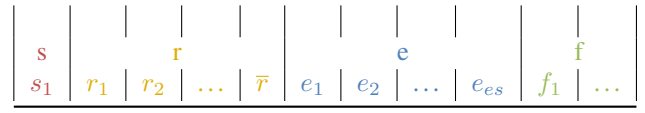


Figure 9. Example posit format.

A.2 Posit Representation

Posit (Gustafson & Yonemoto, 2017; Gustafson, 2017) is a novel real-number representation that is designed as an alternative to the IEEE-754 floating-point (IEEE, 2019).

While an IEEE-754 float consists of a sign bit and a fixed number of bits for mantissa and exponent, the posit representation consists of 4 sections - the sign-bit (s), the regime bits (r), the exponent bits (e) and the fraction bits (f) - where the last three sections have a dynamic number of bits assigned to them, out of the overall fixed number of bits per posit.

The sign bit denotes the sign of the number, where a 0 denotes a positive number and a 1 denotes a negative number. The regime bits, which signify a super-exponent, define a regime value k , which can be positive, negative or zero:

- Positive regime values are represented by a stream of 1s delimited by a single 0. The value of the regime would be one less than the number of leading 1s. For example, if the regime bits are 1110, then $k = 2$; 11111 in a posit with only 6 bits would correspond to $k = 4$.
- Negative regimes are represented by a stream of 0s delimited by a single 1. The value of the regime in this would be $k = -1 \times p$ where p is the number of leading 0s. For example, if the regime bits are 00001, then $k = -4$; 000000 in a posit with only 7 bits would correspond to $k = -6$.
- The value zero is represented by the regime being 10.

The length of the regime is dynamic, and is determined by the number of bits observed till a delimiting bit is encountered. Hence for an n -bit posit, there can be a minimum of 2 and a maximum of $n - 1$ regime bits, (all bits excluding the sign bit). Therefore, the value of k can range from $-(n - 1)$ to $(n - 2)$ in an n -bit number. For a given bitwidth, the es value signifies the maximum number of bits available for the exponent section. Once the sign, regime and exponent bits have been considered, only then the remaining bits are interpreted as fraction bits.

To find the value of a number in posit representation, we define a parameter called *useed* ($= 2^{2^{es}}$). The value of a posit with sign-bit s is

$$(-1)^s \times (\text{useed})^k \times 2^E \times 1.F$$

where E is the value of the exponent represented by the exponent bits (e), k is the value denoted by the regime bits r , and F is the fraction represented by the fraction bits f .

It is possible in the posit representation for a number to contain no exponent bits and/or no fraction bits. In those cases the corresponding values of exponent (E) and fraction (F) are 0.

For example, assuming $es = 2$ and a bitwidth of 8 bits, a bit string 01101101 will be interpreted as:

- Sign bit ($s = 0$).
- Regime bits ($r = \{110\}$). Hence $k = 1$.
- Exponent bits ($e = \{11\}$). Hence $E = 2^3 = 8$.
- Fraction bits ($f = \{01\}$). Hence $1.F = 1.25$.

Since $used = 2^{2^{es}} = 16$, thus the real number represented by our bit string is $1 \times 16^1 \times 8 \times 1.25 = 160$.

A.3 ML and Computer Vision Preliminaries

In this paper, we focus on two broad paradigms of ML problem space: classification and localization (commonly known as detection).

Classification-based models aim to predict singular discrete labels. For example, one can design a classifier which takes as input an image, and predicts a label indicating whether a human is present in the picture or not. The performance of such a model can be objectively measured using classification accuracy, which is the percentage of times the label is correct.

Localization-based models aim to predict more continuous outputs which determine the location of an instance. For example, given the image of a human being, one might need to employ a detection model in order to obtain the bounding-box coordinates of the human being in the picture frame. However, this makes the performance of the model continuous in terms of output quality. We use *Mean Average Precision (MAP)* scores in such a scenario. MAP measures the mean area under the precision-recall curves, and is a standard metric for localization problems like face detection.

ML implementations typically choose the floating-point representation. However, different number representations offer salient advantages, in terms of computation, memory footprint and performance. As such, the effectiveness of a model expressed in a specific number representation is judged by how well it performs compared to its floating-point counterpart.

A.4 Microcontrollers

Microcontrollers, designed for embedded applications, are a class of small, low-power computers on a single integrated circuit (IC). They comprise one or more CPU cores, with some memory and I/O peripherals. Two different kinds of memory are commonly used with microcontrollers, a reprogrammable *read-only* memory for storing firmware called Flash (similar to ROM, EPROM or EEPROM for

personal computers) and a read-write memory called RAM (employing SRAM technology). Microcontrollers allow the storage of read-only bits such as model weights and the compiled software binaries on the Flash, and use their RAM for storing the mutable temporary variables corresponding to the results of intermediate computations. On these devices, RAM is a much more scarce resource than the Flash memory, with the latter often being user-expandable. Additionally, low-end commodity microcontrollers don't even employ hardware caches.

B WORKING EXAMPLE

To motivate the problem addressed in this paper, we provide an exemplar linear classifier model and generate the posit code for it. Consider **Procedure 1**.

Procedure 1: Linear Classifier

$$W_1 := (-2.139562 \quad 1.885351)$$

$$X_1 := \begin{pmatrix} 1.185109 \\ -2.206466 \end{pmatrix}$$

$$B_1 := (0.146048)$$

$$\text{return } (W_1 \times X_1) + B_1$$

Let us set a constraint for running this program in 3 bytes of peak RAM consumption. Here, we assume $W_1 \in \mathbb{R}^{1 \times 2}$, $X_1 \in \mathbb{R}^{2 \times 1}$ and $B_1 \in \mathbb{R}$ are read-only tensors. Hence, they are stored and fetched directly from the Flash, and do not count towards RAM usage. Additionally, we assume that the only two bitwidth options available to us are 8 bits and 16 bits. The corresponding 16-bit *homogeneous* (all tensors assigned the same bitwidth) posit code is depicted in **Procedure 2**. Here, only the temporary tensors t_1 and t_2 are stored in RAM.

Procedure 2: 16-bit Homogeneous Posit ($es=2$) Code

$$\text{posit}_{16}[1][2]W_1 := (-2.13965_{16} \quad 1.88525_{16})$$

$$\text{posit}_{16}[2][1]X_1 := \begin{pmatrix} 1.18506_{16} \\ -2.20605_{16} \end{pmatrix}$$

$$\text{posit}_{16}[1][1]B_1 := (0.146057_{16})$$

$$\text{posit}_{16} \ t_1, t_2;$$

$$t_1 = (W_1 \times X_1)$$

$$t_2 = t_1 + B_1$$

$$\text{return } t_2$$

We observe that the homogeneous 16-bit program uses 4 bytes of RAM (because of t_1 and t_2 being 2 bytes each), making it unsuitable for our target platform. While homogeneous 8-bit code would only take 2 bytes of RAM, and satisfy our memory constraint, it might lead to excessive losses in accuracy. Hence, we make use of *heterogeneous*

bitwidth configurations for our tensors, which use 8-bit for some tensors and 16-bit for others, to reduce RAM consumption, while aiming to minimize the accuracy loss.

HAUNTER defines a promotability score for each tensor (Table 5 and Section 4.1.2). Ranking tensors in the decreasing order of promotability scores gives us an order list of promotion priority for the different tensors in the program.

Table 5. Variable sizes, values and promotability scores.

Var	16-Bit Values	8-Bit Values	Promotability
W_1	(-2.13965, 1.88525)	(-2.25, 1.875)	0.00513
B_1	0.146057	0.140625	0.00543
X_1	(1.18506, -2.20605)	(1.125, -2.25)	0.02198
t_1	-6.69531	-7	0.30469
t_2	-6.54883	-7	0.45117

Table 6. Cumulative promotion within memory limit with different initial states chosen by HAUNTER. Repeated instances have been omitted for brevity.

Promoted Vars	RAM Usage	Error
<i>None</i>	2	0.45047
t_2	3	
t_2, t_1	4	
t_2, X_1	3	
t_2, X_1, B_1	3	
t_2, X_1, B_1, W_1	3	0.19601
t_1	3	
t_1, t_2	4	
t_1, X_1	3	
t_1, X_1, B_1	3	
t_1, X_1, B_1, W_1	3	0.04953
t_2, t_1, X_1, B_1, W_1	4	
t_1, X_1, B_1, W_1	3	0.04953
\vdots		

Procedure 3: Heterogeneous Posit ($es=2$) Code; t_2 uses 8-bits, rest use 16-bits

$$\text{posit}_{16}[1][2]W_1 := (-2.13965_{16} \quad 1.88525_{16})$$

$$\text{posit}_{16}[2][1]X_1 := \begin{pmatrix} 1.18506_{16} \\ -2.20605_{16} \end{pmatrix}$$

$$\text{posit}_{16}[1][1]B_1 := (0.146057_{16})$$

$\text{char}_8[3] \text{ scratch};$

$$\text{scratch}[0 : 1] = \text{posit}_{16}(W_1 \times X_1)$$

$$\text{scratch}[2] = \text{posit}_8(\text{scratch}[0 : 1] + B_1)$$

return $\text{scratch}[2]$

Based on this promotion order, HAUNTER considers a few broad cases suitable for exploration, while starting from different initial configurations, as depicted in Table 6, and explained in Section 4.1.3. At each step of an exploration instance, HAUNTER promotes a tensor cumulatively (i.e. in a successive operation on top of the previous bitwidth configuration), while strictly maintaining the constraint on the RAM consumption, and reverting the promotion in cases where the constraint is violated. At the end of each exploration instance, HAUNTER executes code on the derived bitwidth configuration, and records the accuracy.

Taking the example of the second instance from Table 6, we initiate an exploration with all the tensors being assigned a low bitwidth. Then, based on the promotion order (i.e. $[t_2, t_1, X_1, B_1, W_1]$), we promote t_2 and generate the code on the new bitwidth configuration in order to estimate its RAM usage. We continue promoting other tensors in the promotion order, while keeping the previous tensors in the promoted state, till we end up promoting a tensor which leads to an overshoot of the memory limit (t_1). At this stage, we simply revert the promotion of the ‘‘overshooting’’ tensor, and continue to consider other tensors, till we have exhausted our promotion order. Once we have considered all tensors, we simply execute the generated code and record the accuracy.

Finally, HAUNTER chooses the configuration incurring the minimum loss in accuracy, and generates the final code based on this bitwidth configuration which keeps t_2 as an 8-bit posit and the rest remain as 16-bit posits. During memory management, the RAM tensors are mapped to indices into a global array called *scratch* (Procedure 3) that resides in the RAM. This reduces the runtime overhead of allocating/deallocating tensors during program execution to zero. The RAM usage of the program at runtime is upper-bounded by the size of *scratch*. Here, t_1 occupies the first two bytes, t_2 occupies the third byte of *scratch*, and the RAM consumption of Procedure 3 remains below 3-bytes, as desired.

C HAUNTER: ADDITIONAL DETAILS

C.1 Complexity Analysis: Additional Details

We denote the amount of time required per code generation call as $\mathcal{T}_{codegen}$, and treat it as the upper bound of the code generation and compilation time required for different bitwidth configurations. We follow the same terminology for execution call latency (per example) as well, terming it $\mathcal{T}_{execution}$.

The bitwidth assignment mechanism of SHIFTRY follows an exploration phase where code generation, compilation and execution occurs twice per each tensor, once during individual tensor demotion, and once during cumulative

tensor demotion. Hence for a model with N tensors and supplied with a dataset of D samples, SHIFTRY incurs a cost of $\mathcal{O}(N)$ code generation and $\mathcal{O}(N)$ execution calls, resulting in a bitwidth exploration latency of:

$$\mathcal{O}(N \times \mathcal{T}_{codegen} + N \times D \times \mathcal{T}_{execution})$$

For large models, supplied with large datasets, the second

Algorithm 4: Determining es through accuracy.

Function Preprocess ($lowBitwidth, highBitwidth$):

```

1  if lowBitwidth == 8 then
2      es8 = 2
3       $\rho \leftarrow \{var \mapsto 8\} \forall var \in allVars$ 
      # Generate, compile and execute model code with the
      given set of parameters.
4      accuracyES0  $\leftarrow$ 
        Compile&Execute ( $es = 0, \rho$ )
5      accuracyES2  $\leftarrow$ 
        Compile&Execute ( $es = 2, \rho$ )
6      if accuracyES0 > accuracyES2 then
7          es8 = 0
8  if highBitwidth == 16 then
9      es16 = 2
10      $\rho \leftarrow \{var \mapsto 16\} \forall var \in allVars$ 
11     accuracyES1  $\leftarrow$ 
        Compile&Execute ( $es = 1, \rho$ )
12     accuracyES2  $\leftarrow$ 
        Compile&Execute ( $es = 2, \rho$ )
13     if accuracyES1 > accuracyES2 then
14         es16 = 1
15 return es8, es16
    
```

Algorithm 5: Generating value maps for each bitwidth.

Function

```

CreateValueMaps ( $lowBitwidth, highBitwidth$ ):
1   $\rho \leftarrow \{var \mapsto highBitwidth\} \forall var \in allVars$ 
   # Clear logger file used for storing tensor values.
2  ClearLogs ()
3  accHigh  $\leftarrow$  Compile&Execute ( $\rho$ )
   # Create value map from logged data.
4  varsValueMapHigh  $\leftarrow$  Log&SaveValues ()
5   $\rho \leftarrow \{var \mapsto lowBitwidth\} \forall var \in allVars$ 
6  ClearLogs ()
7  accLow  $\leftarrow$  Compile&Execute ( $\rho$ )
8  varsValueMapLow  $\leftarrow$  Log&SaveValues ()
   # Save accuracy and bitwidth configuration information.
9  SaveAcc&Bitwidth ( $accLow, \rho$ )
10 return varsValueMapLow, varsValueMapHigh
    
```

term is dominant, since $\mathcal{T}_{execution}$ becomes more expensive than $\mathcal{T}_{codegen}$. HAUNTER focuses on reducing the number of execution calls on average to $\mathcal{O}(\log N)$, thereby significantly reducing exploration latency.

The core observation that guides our average case analysis is that most ML models portray an asymmetric diversity in the

tensor sizes. While classification or localization-based models try to “downsize” the input into smaller activations (by some multiplicative factor) at each step, generative models aim to “upsize” the input into larger activations. Empirically, for our benchmarks, the tensor sizes appear to follow an exponential distribution. With that assumption, a constant parameter $\alpha > 1$, and $memoryLimit = C$, for some positive scalar $C = \Theta(N^\alpha) \ll \alpha^N$, we observe that the maximum number of tensors being, safely and cumulatively, promotable to a higher bitwidth is:

$$\lfloor \log (memoryLimit) \rfloor = \lfloor \log C \rfloor = \mathcal{O}(\log N)$$

Algorithm 6: Generating heat map, given the value maps, and promotion order list.

Function CreateHeatMap ($varsValueMapLow, varsValueMapHigh$):

```

1  heatMap = {}
2  for var  $\in allVars$  do
3      lowValues  $\leftarrow$  varsValueMapLow[var]
4      highValues  $\leftarrow$  varsValueMapHigh[var]
5      errors  $\leftarrow$  []
6      for lowValue, highValue  $\in$ 
       {lowValues, highValues} do
7          absError = |highValue - lowValue|
8          error.append(absError)
9      heatMap[var]  $\leftarrow$ 
        Get95thPercentileValue (errors)
         $\div$  varsToSizeMap[var]
10 promotionOrder  $\leftarrow$ 
        DecreasingArgSort (heatMap).keys()
11 return heatMap, promotionOrder
    
```

Algorithm 7: Helper function of Algorithm 8; promoting all variables to high bitwidth subject to memory limit and soft limit factor.

Function

```

PromoteWithinMemoryLimit ( $promotionOrder, memoryLimit, softLimitFactor$ ):
1  overshootingVars  $\leftarrow$  []
2  for var  $\in promotionOrder$  do
3       $\rho \leftarrow \{var \mapsto highBitwidth\}$ 
       # Generate and compile model code for the given
       configuration.
4      memoryUsage  $\leftarrow$  Compile ( $\rho$ )
5      if memoryUsage >
        memoryLimit  $\times$  softLimitFactor then
6           $\rho \leftarrow \{var \mapsto lowBitwidth\}$ 
7      if memoryUsage  $\geq$ 
        memoryLimit  $\times$  softLimitFactor then
8          overshootingVars.append(var)
9  return overshootingVars
    
```

Hence, irrespective of the promotion order and the size of the *overshootingVars* set in **Algorithm 8**, only $\mathcal{O}(\log N)$

number of variables are able to proceed beyond line 10, leading to an average case of $\mathcal{O}(N \log N)$ code generation calls and $\mathcal{O}(\log N)$ execution calls in total. The total bitwidth exploration latency becomes:

$$\mathcal{O}(N \times \log N \times \mathcal{T}_{codegen} + \log N \times D \times \mathcal{T}_{execution})$$

Algorithm 8: HAUNTER Promotion Algorithm

Function PromotionAlgorithm(*promotionOrder*, *memoryLimit*, *softLimitFactor*):

```

1   $\rho \leftarrow \{var \mapsto lowBitwidth\} \forall var \in allVars$ 
2  overshootingVars  $\leftarrow$ 
   PromoteWithinMemoryLimit(promotionOrder,
   memoryLimit, softLimitFactor)
3  accuracy  $\leftarrow$  Compile&Execute( $\rho$ )
4  SaveAcc&Bitwidth(accuracy,  $\rho$ )
5
6  for promotable  $\in$  overshootingVars do
7       $\rho \leftarrow \{var \mapsto lowBitwidth\} \forall var \in allVars$ 
8       $\rho \leftarrow \{promotable \mapsto highBitwidth\}$ 
9      memoryUsage  $\leftarrow$  GetMemoryUsage( $\rho$ )
10     if memoryUsage  $>$ 
11         memoryLimit  $\times$  softLimitFactor then
12              $\left|$  continue
13         PromoteWithinMemoryLimit(promotionOrder,
14         memoryLimit, softLimitFactor)
15         accuracy  $\leftarrow$  Compile&Execute( $\rho$ )
16         SaveAcc&Bitwidth(accuracy,  $\rho$ )
17
18      $\rho \leftarrow \{var \mapsto lowBitwidth\} \forall var \in allVars$ 
19      $\rho \leftarrow \{var \mapsto highBitwidth\} \forall var \in$ 
20         overshootingVars
21     PromoteWithinMemoryLimit(promotionOrder,
22     memoryLimit, softLimitFactor)
23     accuracy  $\leftarrow$  Compile&Execute( $\rho$ )
24     SaveAcc&Bitwidth(accuracy,  $\rho$ )
25
26      $\rho \leftarrow$ 
27         FindBitwidthConfigWithBestAccuracy()
28 return  $\rho$ 

```

This reduction in execution calls becomes significant even for moderately-sized models such as the Face-B model, described in Section 6.2, having 135 tensors, running on a dataset of 405 QVGA images. In our experiments, we observed the exploration time get cut from 49 minutes using SHIFTRY-FIXED to 32 minutes using MINUN-FIXED (Table 12 in Appendix D).

D EVALUATION DETAILS

We now provide detailed results from all of our experiments.

Table 7 summarizes the architecture of the face detection models evaluated in our experiments. All of our face detection models comprise more than one inverted bottleneck residual blocks, commonly called *MBCConv* (see Fig. 3b of (Sandler et al., 2018)). Each *MBCConv* layer consists of three convolution operations executed sequentially:

- C1: A point-wise convolution which expands the number of channels from c_{in} to $c_{in} \times t$, where t is the expansion factor.
- C2: A depth-wise separable convolution with kernel size of 3×3 and stride of either 1 or 2.
- C3: A point-wise convolution which reduces the number of channels in the intermediate tensor from $c_{in} \times t$ to c_{out} .

Table 8 provides accuracy values on different datasets, while comparing different 8-bit representations against the FLOAT32 gold standard. For certain cases, the data-driven scale assignment mechanism of SHIFTRY is unable to determine the appropriate scales for 8-bit fixed-point numbers, and such instances are removed while calculating average accuracy drops. These results show that 8-bit representations suffer from large losses in accuracy.

Table 9 provides accuracy and RAM consumption values on different datasets, while comparing different 16-bit representations, and the FLOAT32 gold standard against MINUN-POSIT. The table shows that MINUN-POSIT suffers from negligible differences in accuracy compared to FLOAT32, while achieving significant reduction in peak RAM consumption, even compared to FIXED16 or BFLOAT16.

Table 10 and Table 11 provide accuracy and RAM consumption values of different bitwidth assignment mechanisms for fixed-point and posit representation respectively. In both of these experiments, we set the RAM consumption of SHIFTRY’s result as the memory limit for the other strategies. In case of MINUN’s result, we provide the RAM consumption values while employing the first-fit greedy heuristic, as well as the optimum memory management using Algorithm X. This evaluation shows that MINUN has better accuracy while consuming less memory than the baselines. Of particular interest is the FACE-B model in Table 10 where optimum RAM management reduces the RAM usage from 218 KBs to 165 KBs.

Table 12 (summarized by Table 3) provides the inference latency and compilation time of different models, on codes generated by SHIFTRY-FIXED and MINUN-FIXED corresponding to Table 10 (summarized by Table 1). Inference latency for classification and localization models has been generated on Arduino Due (84 MHz, 96 KB SRAM, 512 KB Flash) and STM32H747 (240 MHz, 1 MB SRAM, 2 MB Flash) boards respectively. This evaluation shows that the reduction in RAM usage by MINUN does not degrade latency on microcontrollers. Table 13 provides the inference latency obtained on Arduino Uno (16 MHz, 2 KB SRAM, 32 KB Flash) for MINUN-FIXED experiments.

Table 7. Architecture schematics of face detection models. Each line denotes a sequence of layers, repeated n times. The first layer of each MBCConv sequence has stride s and rest use stride 1. Expansion factor t is multiplied to the input channels to change the width. The number of output channels is c .

Input	Layer	t	c	n	s
$320 \times 240 \times 1$	Conv2D 3×3	1	4	1	2
$160 \times 120 \times 4$	RNNPool	1	64	1	4
$40 \times 30 \times 64$	MBCConv	2	32	1	1
$40 \times 30 \times 32$	MBCConv	2	32	7	1
$40 \times 30 \times 32$	MBCConv	2	96	1	2
$20 \times 15 \times 96$	MBCConv	2	96	2	1
$20 \times 15 \times 96$	MBCConv	2	128	1	1
$20 \times 15 \times 128$	MBCConv	2	128	2	1

Table 7. The architecture of Face-A.

Input	Layer	t	c	n	s
$320 \times 240 \times 1$	Conv2D 3×3	1	4	1	2
$160 \times 120 \times 4$	RNNPool	1	64	1	8
$20 \times 15 \times 64$	MBCConv	2	32	1	1
$20 \times 15 \times 32$	MBCConv	2	96	1	1
$20 \times 15 \times 96$	MBCConv	2	96	1	1
$20 \times 15 \times 96$	MBCConv	2	128	1	1

Table 7. The architecture of Face-B.

Input	Layer	t	c	n	s
$320 \times 240 \times 1$	Conv2D 3×3	1	4	1	2
$160 \times 120 \times 4$	RNNPool	1	64	1	4
$40 \times 30 \times 64$	MBCConv	2	32	1	1
$40 \times 30 \times 32$	MBCConv	2	32	1	1
$40 \times 30 \times 32$	MBCConv	2	64	1	2
$20 \times 15 \times 64$	MBCConv	2	64	1	1

Table 7. The architecture of Face-C.

Table 8. Performance of homogeneous 8-bit codes of different representations on FASTGRNN, PROTONN, BONSAI and RNNPOOL models against the FLOAT32 gold standard. Accuracy is in percent. For classification-based models, the number of classes follow the dataset name. An \times in the column indicates that data-driven compilation fails to determine a suitable scale. Average accuracy/MAP drop is calculated with respect to FLOAT32 value.

Model & Dataset	FLOAT32 Accuracy	FIXED8 Accuracy	POSIT8 (Best ES) Accuracy	TFLITE-ZERO-SKEW8 Accuracy
FASTGRNN				
DSA-19	77.76	6.56	69.87	76.56
WAKEWORD-2	98.97	95.66	98.52	84.13
GOOGLE-12	92.99	8.08	44.63	84.42
GOOGLE-30	78.74	4.21	51.57	58.92
HAR-2	91.65	50.87	84.83	88.12
HAR-6	92.03	16.36	91.31	91.89
USPS-10	94.12	52.12	93.92	93.87
MNIST-10	98.05	\times	96.45	12.04
INDUSTRIAL-72	89.96	2.73	81.50	85.69
Average Drop	Base Case	59.96	11.30	15.40
PROTONN				
CIFAR-2	76.45	71.47	66.18	76.64
CR-2	72.91	69.72	66.33	72.85
CR-62	32.74	30.76	31.33	31.75
CURET-61	54.53	39.42	53.10	54.17
LETTER-26	84.02	80.84	82.80	83.50
MNIST-2	95.21	87.40	94.11	95.23
MNIST-10	92.06	85.98	91.23	91.78
USPS-2	94.27	92.58	93.32	94.27
USPS-10	92.53	90.78	91.83	92.73
WARD-2	94.87	77.21	93.42	94.51
Average Drop	Base Case	6.34	2.59	0.22
BONSAI				
CIFAR-2	75.95	73.14	75.90	75.70
CR-2	74.60	72.22	74.97	74.34
CR-62	10.76	9.03	10.76	10.03
CURET-61	45.55	34.50	45.12	44.05
LETTER-26	65.04	60.96	65.28	64.62
MNIST-2	95.96	93.51	95.88	96.03
MNIST-10	93.56	76.32	93.49	93.28
USPS-2	94.82	91.08	94.92	94.67
USPS-10	91.63	89.89	91.83	91.68
WARD-2	95.13	88.30	95.18	94.93
Average Drop	Base Case	5.41	-0.03	0.37
RNNPOOL				
FACE-A	0.643	\times	0.560	\times
FACE-B	0.336	\times	0.209	\times
FACE-C	0.575	5e-5	0.069	3e-5
Average Drop	Base Case	0.575	0.239	0.575

Table 9. Performance of MINUN-POSIT on FASTGRNN, PROTONN, BONSAI and RNNPOOL models against FLOAT32, FIXED16 and BFLOAT16 baselines. Accuracy is in percent, and size is in bytes. For classification-based models, the number of classes follow the dataset name. Average accuracy/MAP drop is calculated with respect to the FLOAT32 value.

Model & Dataset	FLOAT32		FIXED16		BFLOAT16		MINUN-POSIT		
	Accuracy	RAM	Accuracy	RAM	Accuracy	RAM	Accuracy	RAM (OPT)	Bitwidth
FASTGRNN									
DSA-19	77.76	1280	77.70	640	77.59	640	78.00	448	{8, 12}
WAKEWORD-2	98.97	640	98.74	320	98.97	320	99.20	192	{8, 12}
GOOGLE-12	92.99	2000	92.99	1000	92.76	1000	92.83	700	{10, 12}
GOOGLE-30	78.74	2000	78.86	1000	78.76	1000	78.70	750	{8, 12}
HAR-2	91.65	1600	91.52	800	91.55	800	91.55	500	{8, 10}
HAR-6	92.03	1600	92.03	800	91.52	800	91.99	560	{8, 12}
USPS-10	94.12	1664	94.12	832	94.12	832	94.17	448	{8, 10}
MNIST-10	98.05	2560	85.74	1280	98.12	1280	98.10	960	{8, 12}
INDUSTRIAL-72	89.96	1280	89.88	640	89.53	640	89.80	480	{12, 16}
Average Drop	Base Case		0.41		0.15		-0.01		
PROTONN									
CIFAR-2	76.45	312	76.49	156	76.47	156	76.59	70	{8, 12}
CR-2	72.91	412	73.07	206	73.12	206	73.17	94	{8, 12}
CR-62	32.74	552	32.74	276	32.79	276	32.69	171	{8, 12}
CURET-61	54.53	544	54.53	272	54.67	272	54.53	138	{8, 12}
LETTER-26	84.02	308	83.60	154	83.92	154	84.02	81	{8, 12}
MNIST-2	95.21	240	95.23	120	95.25	120	95.30	39	{8, 10}
MNIST-10	92.06	244	92.04	122	92.09	122	92.10	49	{8, 10}
USPS-2	94.27	240	94.27	120	94.32	120	94.47	44	{8, 12}
USPS-10	92.53	3240	92.58	1620	92.58	1620	92.48	800	{8, 9}
WARD-2	94.87	212	94.87	106	94.82	106	94.82	39	{8, 10}
Average Drop	Base Case		0.02		-0.05		-0.06		
BONSAI									
CIFAR-2	75.95	320	75.94	160	75.91	160	75.90	40	{8, 12}
CR-2	74.60	320	74.66	160	74.71	160	74.97	40	{8, 12}
CR-62	10.76	1072	10.81	536	10.76	536	10.76	258	{8, 12}
CURET-61	45.55	1072	45.55	536	45.62	536	45.55	255	{8, 12}
LETTER-26	65.04	496	65.10	248	64.98	248	64.84	114	{8, 12}
MNIST-2	95.96	160	95.96	80	95.96	80	95.98	20	{8, 12}
MNIST-10	93.56	240	93.47	120	93.51	120	93.44	50	{8, 12}
USPS-2	94.82	480	94.82	240	94.82	240	94.92	60	{8, 12}
USPS-10	91.63	304	91.63	152	91.53	152	91.63	45	{8, 12}
WARD-2	95.13	160	95.18	80	95.13	80	95.18	20	{8, 12}
Average Drop	Base Case		-0.01		0.01		-0.02		
RNNPOOL									
FACE-A	0.643	618K	0.628	309K	0.646	309K	0.647	197K	{10, 12}
FACE-B	0.336	614K	0.301	307K	0.335	307K	0.333	192K	{10, 12}
FACE-C	0.575	618K	0.562	309K	0.574	309K	0.573	203K	{10, 12}
Average Drop	Base Case		0.021		0.000		0.000		

Table 10. Performance of MINUN-FIXED on FASTGRNN, PROTONN, BONSAI and RNNPOOL models against computationally expensive bitwidth assignment mechanisms and the previous state-of-the-art. Accuracy is in percent, and size is in bytes. For classification-based models, the number of classes follow the dataset name. Average accuracy/MAP drop is calculated with respect to MINUN-FIXED value.

Model & Dataset	SHIFTRY-FIXED		Accuracy-Based		Size-Based		MINUN-FIXED		
	Accuracy	RAM	Accuracy	RAM	Accuracy	RAM	Accuracy	RAM	RAM (OPT)
FASTGRNN									
DSA-19	74.39	740	77.70	640	77.70	640	77.70	640	640
WAKEWORD-2	98.63	377	98.74	320	98.74	320	98.74	320	320
GOOGLE-12	92.24	1141	92.99	1000	92.99	1000	92.99	1000	1000
GOOGLE-30	78.42	1000	78.86	1000	78.86	1000	78.86	1000	1000
HAR-2	90.09	845	91.52	800	91.52	800	91.52	800	800
HAR-6	90.23	720	90.50	720	90.84	720	88.26	730	720
USPS-10	92.98	512	92.98	512	92.88	512	93.02	512	512
MNIST-10	85.74	1280	85.74	1280	85.74	1280	85.74	1280	1280
INDUSTRIAL-72	87.31	520	87.31	520	87.71	520	87.71	520	520
Average Drop	0.5		-0.2		-0.27		Base Case		
PROTONN									
CIFAR-2	75.18	93	75.65	93	75.43	81	76.16	93	93
CR-2	72.85	124	72.53	124	71.32	106	72.64	124	124
CR-62	31.70	272	31.70	272	31.75	226	32.27	226	226
CURET-61	53.10	146	54.10	145	51.60	138	53.89	145	145
LETTER-26	81.78	77	81.78	77	82.42	77	83.30	77	77
MNIST-2	94.80	60	95.07	60	95.12	60	95.26	60	56
MNIST-10	91.78	61	91.95	61	91.93	61	91.94	61	61
USPS-2	92.83	60	93.92	60	94.02	60	94.07	60	56
USPS-10	91.63	810	91.63	810	92.03	810	92.73	820	800
WARD-2	93.68	63	93.68	63	94.05	63	94.51	63	63
Average Drop	0.74		0.48		0.71		Base Case		
BONSAI									
CIFAR-2	74.60	80	74.60	80	74.89	80	75.08	80	66
CR-2	74.34	100	74.34	100	74.87	100	74.44	100	66
CR-62	9.40	268	9.40	268	9.40	268	9.56	288	268
CURET-61	42.77	524	43.41	524	43.98	524	45.55	536	488
LETTER-26	63.26	124	63.48	108	63.52	108	63.52	122	108
MNIST-2	95.85	50	96.03	50	95.99	50	95.92	50	36
MNIST-10	92.70	60	93.12	60	92.59	60	93.05	60	60
USPS-2	94.07	120	94.07	120	94.12	120	94.37	120	96
USPS-10	91.48	76	91.48	76	91.53	76	91.63	80	72
WARD-2	93.94	50	95.29	50	94.77	50	95.08	50	36
Average Drop	0.58		0.30		0.25		Base Case		
RNNPOOL									
FACE-A	0.338	235K	0.635	213K	0.635	213K	0.626	232K	232K
FACE-B	0.314	218K	0.320	218K	0.320	218K	0.320	218K	165K
FACE-C	0.139	204K	0.548	188K	0.548	188K	0.548	188K	185K
Average Drop	0.233		-0.003		-0.003		Base Case		

Table 11. Performance of MINUN-POSIT on FASTGRNN, PROTONN, BONSAI and RNNPOOL models against computationally expensive bitwidth assignment mechanisms and the previous state-of-the-art. Accuracy is in percent, and size is in bytes. For classification-based models, the number of classes follow the dataset name. Average accuracy/MAP drop is calculated with respect to MINUN-POSIT value.

Model & Dataset	SHIFTRY-POSIT		Accuracy-Based		Size-Based		MINUN-POSIT		
	Accuracy	RAM	Accuracy	RAM	Accuracy	RAM	Accuracy	RAM	RAM (OPT)
FASTGRNN									
DSA-19	77.00	448	77.00	448	76.91	448	77.13	456	448
WAKEWORD-2	98.40	160	98.40	160	98.40	160	98.40	160	160
GOOGLE-12	92.50	941	92.57	941	92.54	941	92.63	900	900
GOOGLE-30	77.31	951	78.64	951	78.35	800	78.65	902	900
HAR-2	90.80	720	91.18	720	91.14	720	91.18	720	720
HAR-6	91.35	400	91.35	400	91.25	400	91.35	400	400
USPS-10	94.02	416	94.02	416	94.17	416	93.82	416	416
MNIST-10	96.68	768	96.68	768	96.86	768	96.83	768	768
INDUSTRIAL-72	86.56	640	89.84	640	89.84	640	89.84	640	640
Average Drop	0.58		0.02		0.04		Base Case		
PROTONN									
CIFAR-2	76.30	79	76.52	79	68.82	51	76.47	79	79
CR-2	73.07	104	72.85	104	66.97	66	72.80	104	104
CR-62	32.12	136	32.53	136	31.44	136	32.43	136	135
CURET-61	53.10	134	54.17	134	53.10	134	54.17	134	133
LETTER-26	82.62	64	82.62	64	82.62	64	82.70	64	63
MNIST-2	93.93	40	93.93	40	94.67	40	94.86	40	33
MNIST-10	91.31	41	91.31	41	91.37	41	91.62	41	41
USPS-2	93.17	40	93.17	40	94.02	40	94.07	40	36
USPS-10	91.83	810	92.83	810	92.43	810	92.53	820	800
WARD-2	94.41	54	94.98	54	93.79	36	94.93	54	54
Average Drop	0.47		0.17		1.73		Base Case		
BONSAI									
CIFAR-2	75.90	40	75.67	40	75.96	40	75.90	40	40
CR-2	74.97	40	74.66	40	74.76	40	74.97	40	40
CR-62	10.76	268	10.50	268	10.76	268	10.76	268	248
CURET-61	45.12	268	45.69	268	45.47	268	45.76	268	256
LETTER-26	65.28	124	65.26	118	65.08	118	65.28	124	104
MNIST-2	95.88	20	95.88	20	96.06	20	96.03	20	20
MNIST-10	93.49	50	93.43	50	93.49	50	93.49	50	50
USPS-2	94.92	60	94.77	60	94.92	60	94.92	60	60
USPS-10	91.83	48	91.73	48	91.83	48	91.83	48	44
WARD-2	95.18	20	95.18	20	95.18	20	95.18	20	20
Average Drop	0.08		0.14		0.06		Base Case		
RNNPOOL									
FACE-A	0.583	235K	0.638	213K	0.638	213K	0.640	230K	230K
FACE-B	0.297	230K	0.297	230K	0.297	230K	0.331	230K	230K
FACE-C	0.464	230K	0.464	230K	0.464	230K	0.464	230K	230K
Average Drop	0.030		0.012		0.012		Base Case		

Table 12. Inference time and compilation time of MINUN-FIXED on FASTGRNN, PROTONN, BONSAI and RNNPOOL models. Inference values are in seconds, and compilation breakup is presented as a percentage of the overall compilation cost. Inference values are obtained by averaging over the final test set. For classification-based models, the number of classes follow the dataset name.

Model & Dataset	SHIFTRY-FIXED		MINUN-FIXED				
	Time(s)		Time(s)		Compilation Breakup (%)		
	Inference	Compiler	Inference	Compiler	Stage I & II	Stage III	Section 4.3
FASTGRNN							
DSA-19	1.964	919.77	2.047	552.6	94.54	5.45	0.01
WAKEWORD-2	1.167	429.27	1.124	242.2	91.52	8.46	0.02
GOOGLE-12	2.645	717.12	2.718	443.2	94.44	5.53	0.03
GOOGLE-30	3.043	701.65	3.060	427.2	91.64	8.32	0.04
HAR-2	2.690	288.72	2.633	143.4	89.96	10.02	0.02
HAR-6	3.201	289.90	2.990	160.9	81.96	18.01	0.03
USPS-10	1.094	183.42	1.172	106.7	68.22	31.76	0.02
MNIST-10	0.901	1765.29	0.903	1026.5	99.52	0.47	0.01
INDUSTRIAL-72	0.092	240.55	0.092	115.2	76.43	23.51	0.06
PROTONN							
CIFAR-2	0.003	387.08	0.004	275.36	84.48	15.50	0.02
CR-2	0.006	100.07	0.007	64.72	72.17	27.78	0.05
CR-62	0.008	100.94	0.007	65.52	72.29	27.62	0.09
CURET-61	0.007	112.35	0.008	73.93	74.33	25.55	0.12
LETTER-26	0.010	94.72	0.010	60.36	68.45	31.45	0.10
MNIST-2	0.004	846.66	0.004	574.83	87.30	12.69	0.01
MNIST-10	0.004	857.41	0.004	570.29	87.39	12.60	0.01
USPS-2	0.003	116.36	0.003	69.11	73.25	26.71	0.04
USPS-10	0.004	112.52	0.005	65.39	79.63	20.30	0.07
WARD-2	0.004	136.06	0.005	92.33	77.50	22.46	0.04
BONSAI							
CIFAR-2	0.002	777.45	0.002	434.16	89.69	10.30	0.01
CR-2	0.002	211.18	0.002	89.89	77.15	22.82	0.03
CR-62	0.010	153.44	0.010	78.37	83.78	16.10	0.12
CURET-61	0.013	162.71	0.015	84.04	84.19	15.48	0.33
LETTER-26	0.004	127.07	0.005	71.66	65.60	34.34	0.06
MNIST-2	0.002	1469.21	0.003	823.83	91.21	8.78	0.01
MNIST-10	0.004	1284.33	0.005	774.28	87.55	12.44	0.01
USPS-2	0.002	220.63	0.002	92.87	77.81	22.15	0.04
USPS-10	0.003	172.82	0.003	99.00	80.54	19.43	0.03
WARD-2	0.003	237.05	0.003	121.28	82.16	17.82	0.02
RNNPOOL							
FACE-A	16.661	9279.46	16.864	11265.9	37.21	61.46	1.33
FACE-B	7.880	2955.20	7.942	2343.09	55.50	26.61	17.89
FACE-C	9.440	3060.02	9.140	2039.10	68.24	30.71	1.05

Table 13. Inference time of MINUN-FIXED on Arduino Uno board for FASTGRNN, PROTONN and BONSAI models. Inference values are in seconds, and are obtained by averaging over the final test set. The number of classes follow the dataset name.

Model & Dataset	MINUN-FIXED Time(s) Inference
FASTGRNN	
DSA-19	56.18
WAKEWORD-2	27.61
GOOGLE-12	75.18
GOOGLE-30	98.72
HAR-2	93.48
HAR-6	94.38
USPS-10	2.70
MNIST-10	25.89
INDUSTRIAL-72	1.70
PROTONN	
CIFAR-2	0.07
CR-2	0.13
CR-62	0.27
CURET-61	0.07
LETTER-26	0.20
MNIST-2	0.10
MNIST-10	0.11
USPS-2	0.05
USPS-10	0.11
WARD-2	0.11
BONSAI	
CIFAR-2	0.08
CR-2	0.08
CR-62	0.31
CURET-61	0.36
LETTER-26	0.07
MNIST-2	0.08
MNIST-10	0.09
USPS-2	0.08
USPS-10	0.04
WARD-2	0.10